Computers and Chemical Engineering 72 (2015) 3–20

Contents lists available at ScienceDirect

Computers and Chemical Engineering

journal homepage: www.elsevier.com/locate/compchemeng

A framework for efficient large scale equation-oriented flowsheet optimization

Alexander W. Dowling, Lorenz T. Biegler*

Chemical Engineering Department, Carnegie Mellon University, Pittsburgh, PA 15213, United States

ARTICLE INFO

Article history:
Received 20 January 2014
Received in revised form 12 May 2014
Accepted 13 May 2014
Available online 27 May 2014

Keywords:
Process optimization
Heat integration
Distillation
Air separation unit
Coal oxycombustion
Mathematical programming with complementarity constraints

ABSTRACT

Despite the economic benefits of flowsheet optimization, many commercial tools suffer from long computational times, limited problem formulation flexibility and numerical instabilities. In this study, we address these challenges and present a framework for efficient large scale flowsheet optimization. This framework couples advanced process optimization formulations with state-of-the-art algorithms, and includes several notable features such as (1) an optimization-friendly formulation of cubic equation of state thermodynamic models; (2) a new model for distillation column optimization based on rigorous mass, equilibrium, summation and heat (MESH) equations with a variable number of trays that avoids integer variables; (3) improvements on the Duran–Grossmann formulation for simultaneous heat integration and flowsheet optimization; and (4) a systematic initialization procedure based on model refinements and a tailored multi-start algorithm to improve feasibility and identify high quality local solutions.

Capabilities of the framework are demonstrated on a cryogenic air separation unit synthesis study, including two thermally coupled distillation columns and accompanying multistream heat exchangers. A superstructure is formulated that includes several common ASU configurations in literature. As part of the optimization problem the solver selects the best topology in addition to operating conditions (temperatures, flowrates, etc.) for coal oxycombustion applications. The optimization problem includes up to 16,000 variables and 500 degrees of freedom, and predicts specific energy requirement of 0.18 to 0.25 kWh/kg of O_2 depending on design assumptions. These results are compared to literature and plans to extend the framework to an entire coal oxycombustion power plant optimization study are discussed.

1. Introduction

Flowsheet optimization and synthesis improve process designs by systematically exploring nearly uncountable process configurations. By facilitating the selection of the best designs, optimization ultimately reduces costs, increases efficiency and improves plant operability. Applied to tomorrow's power systems, large scale optimization will help reduce the capital and operational costs of carbon capture, utilization and sequestration. Furthermore, optimization frameworks allow for an automated, systematic screening of promising technologies, ranging from single systems, such as membranes for CO_2 separation, to entire new flowsheets, such as coal oxycombustion. As a result, they provide insight to the potential value of new technologies throughout the development cycle.

Equation oriented (EO) approaches offer several advantages over more traditional sequential modular (SM) methods for simulation. Sequential modular methods work by simulating each unit (module) individually and then converging the entire flowsheet with a combination of iterations and heuristics. In contrast, equation oriented methods apply Newton's method for solving systems of nonlinear equations to simulate the flowsheet, enabling simultaneous optimization and convergence of the flowsheet. More generally, EO formulations directly exploit advances in mathematical programming development, leading to distinct advantages over SM methods with regards to optimization, including:

- **Efficient large scale solvers:** The availability of accurate first and second derivative information calculated via automatic differentiation enables the use of very efficient large scale nonlinear programming algorithms, capable of handling 100,000+ constraints and equations (including inequality constraints). Optimization algorithms available in SM packages (such as SQP

* Corresponding author. Tel.: +1 412 268 2232; fax: +1 412 268 7139.
E-mail addresses: biegler@cmu.edu, lb01@andrew.cmu.edu (L.T. Biegler).

http://dx.doi.org/10.1016/j.compchemeng.2014.05.013
0098-1354/

methods) cannot handle these large problems and typically experience convergence difficulties due to inaccurate derivative information. Alternately derivative free methods (genetic algorithms, particle swarm, etc.) are commonly used with SM approaches. These algorithms, however, are less efficient and may not provide guarantees that their results are optimum.

- **Modeling discrete events and decisions:** Many process synthesis tasks require modeling discrete events and decisions. These can be accommodated in EO frameworks with disjunctive programming and mixed integer nonlinear programming (MINLP) algorithms. Furthermore, some discrete variables can be replaced with smoothing functions or complementarities (Dowling and Biegler, 2013; Kraemer et al., 2009; Stein et al., 2004), another active area of mathematical programming research. As discussed in Section 4, the solution of non-convex MINLPs is not without it challenges. However, optimization of discrete variables with SM methods remains extremely challenging, as provable convergence to a local optimum is difficult to demonstrate.
- **Optimization decomposition methods:** EO modeling allows the use of powerful decomposition methods (Lagrangian, Schur complement, etc.) that break the original problem into more manageable subproblems. See Zhu et al. (2010, 2011) for examples of decomposition methods applied to very large scale process design problems under uncertainty.
- **Low cost sensitivity analysis:** Using EO methods, sensitivity information at the optimal solution is available as a byproduct of the solution procedure; KKT multipliers report the linearized sensitivity of the objective function with respect to perturbations in each bound and constraint. This information is especially valuable in process optimization studies, where one may be forced to rely on assumptions or weakly validated models that constrain the optimal value. In contrast performing sensitivity analysis around a solution with SM methods requires simulating the flowsheet at multiple design points around the optimal solution.

See Biegler et al. (1997) for further discussion of SM and EO flowsheeting methods.

Many opportunities exist for advancement of EO flowsheet methods, such as the development of robust initialization procedures, the refinement of optimization formulations to avoid integer variables and the application of decomposition methods for design under uncertainty. Tackling these challenges requires development of environments for EO flowsheet optimization that extend beyond existing commercial tools, both in terms of modeling flexibility and the ability to interface with numerous optimization algorithms. In this paper we present a new EO optimization framework and demonstrate its capabilities with a cryogenic air separation unit (ASU) synthesis study.

Two central themes are present throughout the framework: (1) refinement for robust initialization, and (2) modular equation-oriented models. Regarding initialization, the flowsheet is first optimized using simplified models for each core module. The simplified solutions are then used to initialize the more detailed (and difficult to optimize) models, resulting in an initialization procedure that has been quite successful with the ASU demonstration system. Regarding modularity, many of the units are generalized as thermodynamic equipment (requiring phase equilibrium calculations) or heat exchange equipment. These units inherit (borrowing a concept from computer science) equations from their generalized parent models, resulting in a concise framework that is easy to extend.

The remainder of the paper is organized as follows. First, the four core modules for the framework are introduced. In Section 2 the **thermodynamics module** is discussed. It contains both the ideal gas/correlation-based and the more rigorous cubic equation of state (CEOS) models. Results from optimization with the ideal gas model are used to initialize the CEOS variables. Strategies to accommodate vanishing phases for both models are examined. Next, in Section 3, the thermodynamic models are extended to a **common equipment model**. Refinements of the general model into specific types of units (flash vessels, throttle valves, etc) are discussed. In Section 4, two **models for distillation cascades** are presented. The first is an extension of the shortcut model developed by Kremser and refined by Edmister. The second is a new rigorous MESH model with tray bypass. Both of these approaches avoid integer variables, allowing the distillation models to be solved as a continuous nonlinear system. In Section 5, the Duran–Grossmann pinch based method for simultaneous **heat integration** and process optimization is discussed and modifications are presented. An approach to accommodate phase changes is incorporated, along with a model refinement technique to improve the constant heat capacity assumption. In Section 6 **practical concerns**, such as systematic initialization and avoiding degenerate equations are considered. The new EO framework is demonstrated in Section 7 in a **cryogenic air separation unit design case study** for advanced fossil fuel power plants. Finally, conclusions and future directions are discussed in Section 8.

2. Integrated thermodynamics models

For EO-based optimization, we begin with the underlying thermodynamic models that calculate properties (enthalpy, fugacity, etc.) used in each process stream. Two separate modules are included in the framework. The *simple* module relies on ideal gas assumptions and related correlations, and the second module uses *cubic equation of state* (CEOS) models (specifically Peng–Robinson or Soave–Redlich–Kwong) that are available in many common flowsheet simulators. The results from the simple module are used to initialize the CEOS equations.

The remainder of this section is organized as follows. First, we summarize vapor–liquid calculations with phase disappearance; this defines the strategy to model vanishing phases. Next both thermodynamics modules are introduced, along with a common stream model. Relaxation strategies are then applied to both modules to accommodate phase disappearance. Finally, an EO approach for phase verification is discussed.

2.1. Phase disappearance and VLE calculations

At the heart of optimization-based process synthesis is the concept of formulating a superstructure to simultaneously consider many different system configurations. Inevitably some streams in the superstructure will have no flow. For example, consider a flash vessel where each phase is modeled as a separate outlet stream in equilibrium. Both phases are present under only certain temperature, pressure and feed composition conditions (resulting in both outlet streams with positive flowrates). In all other cases, one of the streams will vanish and the constraints specifying phase and equilibrium relationships must be relaxed. In order to develop a robust VLE model, we start with the Gibbs free energy minimization problem and write the KKT optimality conditions (see Chapter 11 of Biegler (2010) for further details). After some reformulation of the fugacity formulas, the complementarity conditions are written as follows:

$$y_c = \beta K_c x_c \tag{1a}$$

$$-\sigma^L \le \beta - 1 \tag{1b}$$

$$\beta - 1 \le \sigma^V \tag{1c}$$

$$0 \le L \perp \sigma^L \ge 0 \tag{1d}$$

$$0 \le V \perp \sigma^V \ge 0 \tag{1e}$$

Here, K_c is the equilibrium coefficient, given by the ratio of liquid to vapor fugacity and the $\perp$ operator denotes complementarity (at least one of the two sides/arguments must be zero). For example, in Eq. (1d), at least one of the inequalities must be active, thus either $L = 0$ or $\sigma^L = 0$. The coefficient β relaxes the equilibrium calculation ($y_c = K_c x_c$) when one phase vanishes. This is seen by further examining the complementarity conditions. If both phases are present, the slack variables σ^V and σ^L must both be zero, resulting in $\beta = 1$. Likewise if the vapor phase disappears, $\sigma^V \geq 0$ and $\beta \geq 1$, and if the liquid phase disappears $\sigma^L \geq 0$ and $\beta \leq 1$. By using Eq. (1), the Gibbs free energy minimization problem can be efficiently embedded and solved as part of flowsheet calculations. Applications of this formulation are reported in Biegler (2010), Gopal and Biegler (1999).

2.2. Prerequisites: stream model and common equations

A flowsheet is a collection of *streams* and *units* that perform operations to change the streams' properties. These properties include total flowrate F_s, component flowrate $f_{s,c}$, component mole fraction $x_{s,c}$ (or $y_{s,c}$), temperature T_s, pressure P_s, specific molar enthalpy H_s and fugacity $\phi_{s,c}$. Indices s and c represent streams and components, respectively. Additional stream properties are introduced as needed throughout this section. Basic stream model equations are shown below. For vapor streams $y_{s,c}$ is used in place of $x_{s,c}$.

$$F_s = \sum_{c \in \{Comps\}} f_{s,c} \qquad \forall s \in \{Str\} \tag{2}$$

$$f_{s,c} = F_s x_{s,c} \quad \forall c \in \left\{\mathrm{Comp}_1, \ldots, \mathrm{Comp}_{n-1}\right\}, \quad \forall s \in \left\{Str\right\} \tag{3}$$

$$1 = \sum_c x_{s,c} \qquad \forall s \in \{Str\} \tag{4}$$

Both thermodynamic modules share several common equations, including formulas for ideal gas enthalpy (H^{IG}) and scaled temperature (T^*); T^r is reduced temperature constant. T^* is used exclusively in the remaining models; Eq. (5) is excluded from optimization problems and applied in a post processing step to calculate T. We have empirically observed this results in better scaling (nominal variable values near unity) and improves optimizer performance. The coefficients for Eq. (6) are available in Reid et al. (1977).

$$T_s = T_s^* T^r \qquad \forall s \in \{Str\} \tag{5}$$

$$H_s^{IG} = \sum_{c \in \{Comp\}} x_{s,c} \left[\frac{C_c^{\mathrm{V}} (T^r)^5}{5} [(T_s^*)^5 - 1] + \frac{C_c^{\mathrm{IV}} (T^r)^4}{4} [(T_s^*)^4 - 1] + \ldots + C_c^{\mathrm{I}} (T^r)[(T_s^*) - 1] \right] \qquad \forall s \in \{Str\} \tag{6}$$

Various sets are used to manage flowsheet connectivity. $\{Str\}$ is the parent set containing all possible streams in the flowsheet. It is further divided into subsets: $\{LiqStr\}$ and $\{VapStr\}$ contain liquid and vapor streams, respectively, that cannot vanish. In contrast, $\{FlashLiq\}$ and $\{FlashVap\}$ contain liquid and vapor streams used in flash calculations, and these may vanish. Other subsets of $\{Str\}$ are introduced as needed and listed in the nomenclature tables. All of these subsets are automatically populated in the optimization framework depending on the flowsheet connectivity discussed in Section 3.

2.3. Simple thermodynamics module

Optimization with the simple thermodynamics module produces a good initial point for the more rigorous CEOS models. Vapor pressure (P^{vap}) is calculated using the Antoine equation (Eq. (7)). Vapor pressure and vapor–liquid equilibrium are calculated via Raoult's law (Eq. (8)). Phases are determined by calculating bubble and dew point pressures (Eqs. (9) and (10)) from the mixture vapor pressure and examining the stream pressure, as shown in Eqs. (11) and (12). The index g represents thermodynamic equipment, which are discussed in Section 3.

$$P_{s,c}^{vap} = \exp[\mathcal{A}_c^a - \mathcal{A}_c^b/(T_s + \mathcal{A}_c^c)] \tag{7}$$

$$K_{g,c} P_s = P_{s,c}^{vap} \quad s \in \{OutVThrmE\} \tag{8}$$

$$P_s^b = \sum_c x_{s,c} P_{s,c}^{vap} \tag{9}$$

$$P_s^d \sum_c \frac{x_{s,c}}{P_{s,c}^{vap}} = 1 \tag{10}$$

$$P_s \geq P_s^b \qquad s \in \{LiqStr\} \tag{11}$$

$$P_s \leq P_s^d \qquad s \in \{VapStr\} \tag{12}$$

However, because gas enthalpies are independent of pressure the above models cannot predict cooling in throttle valves. As a workaround, we fit correlations for gas and liquid enthalpies from thermodynamic data generated from a cubic EOS. This approach is consistent with the purpose of the simple thermodynamic models, which obtain reasonable results for initialization of rigorous models. Moreover, it avoids explicit consideration (and tuning) of Joule–Thomson equations for valves. For each component in the flowsheet, a large temperature and pressure space was sampled with the Peng Robinson EOS with AspenPlus for pure substances. Eqs. (13) and (14) were fit to the vapor and liquid data, respectively, using linear regression techniques. Stream enthalpies are obtained by assuming ideal mixing as follows:

$$H_{s,c} = \mathcal{H}_{v,c}^1 + \mathcal{H}_{v,c}^2 P_s + \mathcal{H}_{v,c}^3 P_s^2 + \mathcal{H}_{v,c}^4 T_s^* + \mathcal{H}_{v,c}^5 (T_s^*)^2 + \mathcal{H}_{v,c}^6 (T_s^*)^3 + \mathcal{H}_{v,c}^7 T_s^* P_s + \mathcal{H}_{v,c}^8 (T_s^*)^2 P_s, \quad \forall s \in \{VapStr \cup FlashVap\}, \quad \forall c \in \{Comps\} \tag{13}$$

$$H_{s,c} = \mathcal{H}_{l,c}^1 + \mathcal{H}_{l,c}^4 T_s^* + \mathcal{H}_{l,c}^5 (T_s^*)^2 + \mathcal{H}_{l,c}^6 (T_s^*)^3 + \mathcal{H}_{l,c}^7 T_s^* P_s + \mathcal{H}_{l,c}^8 (T_s^*)^2 P_s, \quad \forall s \in \{LiqStr \cup FlashLiq\}, \quad \forall c \in \{Comps\} \tag{14}$$

2.4. Cubic equation of state thermodynamics module

Cubic equations of state (CEOS) are versatile models for process simulation, balancing reasonable accuracy with moderate computational complexity. The models also represent both liquid and vapor phases for non-polar and slightly polar compounds (with appropriate mixing rules and interaction parameters). See Reid et al. (1987) for background material. The most general cubic equation of state is shown in Eq. (15). A and B represent reduced parameters, whose formulas are given in Eqs. (17) and (18). EOS specific values and formulas are given in Table 1. As described in the Supplemental Material, binary interaction parameters are taken from Knapp et al. (1982). T^c and P^c correspond to critical point temperatures and pressures for each component.

$$f(Z) = Z^3 - (1 + B - uB)Z^2 + (A + wB^2 - uB - uB^2)Z - AB - wB^2 - wB^3 = 0 \tag{15}$$

$$Z = \frac{PV}{RT} \tag{16}$$

Table 1
Formulas and parameters for two popular CEOS models (Reid et al., 1987).

	Soave (SRK)	Peng–Robinson (PR)
u	1	2
w	0	-1
b	$\frac{0.08664RT^c}{P^c}$	$\frac{0.07780RT^c}{P^c}$
a	$\frac{\Omega_a R^2(T^c)^2}{P^c}[1+f_\omega(1-\sqrt{T^r})]^2$	
Ω_a	0.42748	0.45724
f_ω	$0.48+1.574\omega-0.176\omega^2$	$0.37464+1.54226\omega-0.26992\omega^2$

$$A = \frac{aP}{R^2T^2} \tag{17}$$

$$B = \frac{bP}{RT} \tag{18}$$

Historically CEOS models have required iterative, non-smooth heuristics for root selection. Kamath et al. (2010) worked around this problem using inequality constraints in an optimization-friendly formulation. These inequality constraints are used to select the appropriate root for each phase (Z_l for liquid, Z_v for vapor) and can be relaxed to accommodate phase disappearance. Eqs. (19) and (20) are the constraints for liquid streams, and Eqs. (21) and (22) correspond to vapor streams:

$$f'(Z_l) = 3Z_l^2 - 2(1+B-uB)Z_l + A + wB^2 - uB - uB^2 \geq 0 \tag{19}$$

$$f''(Z_l) = 6Z_l - 2(1+B-uB) \leq 0 \tag{20}$$

$$f'(Z_v) = 3Z_v^2 - 2(1+B-uB)Z_v + A + wB^2 - uB - uB^2 \geq 0 \tag{21}$$

$$f''(Z_v) = 6Z_v - 2(1+B-uB) \geq 0 \tag{22}$$

In practice Eqs. (19) and (21) are bounded away from zero by a small number, such that $f'(Z) \geq \varepsilon^{CEOS}$. Our experience shows this makes the Jacobian matrix slightly better conditioned, and improves algorithm performance.

This formulation is attractive for four reasons:

1. Cubic equations of state are popular methods for modeling many systems. Input properties and custom interaction models can also be added to the base CEOS framework to handle additional mixtures and extreme conditions.
2. All models are posed in a declarative way as algebraic equality and inequality constraints. They are easy to embed in an optimization modeling environment such as GAMS, AMPL or AIMMS. These models are smooth and differentiable, avoiding heuristics for phase detection commonly used in flowsheet simulators.
3. Many of the optimization modeling environments apply automatic differentiation to obtain accurate first and second derivatives with no additional programming effort.
4. Slack variables can be added to this model to accommodate phase disappearances.

Thermodynamic properties including enthalpy (H), entropy (S) and fugacity (ϕ) are calculated using departure functions and mixing rules from (Reid et al., 1987), as shown in the supplemental material. In general these cubic equation of state models should represent non-polar and slightly polar molecules well enough for basic process design and optimization.

Phase equilibria are calculated by relating the fugacity coefficients for each pair of streams (s^l & s^v) and component (c) exiting every thermodynamic equipment unit (index g), $K_{g,c} = \phi_{s^l,c}/\phi_{s^v,c}$.

2.5. Relaxation of thermodynamic modules

When phases vanish, the equations for phase selection must be relaxed along with the equilibrium condition. Kamath et al. (2010) use slack variables and the big-M formulation to relax Eqs. (20) and (22) from the cubic EOS module to obtain Eqs. (23) and (24).

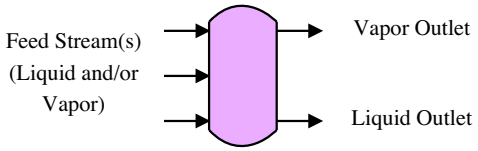

Fig. 1. General and thermodynamic equipment structure.

$$f''(Z_l) = 6Z_l - 2(1+B-uB) \leq M\sigma^L \tag{23}$$

$$f''(Z_v) = 6Z_v - 2(1+B-uB) \geq -M\sigma^V \tag{24}$$

As the slack variables increase from zero, the phase selection constraints are relaxed. This behavior should be allowed only if the corresponding stream flowrate (F_s) is zero, as modeled by a complementarity condition (Eq. (25)). In practice the complementarity condition is accommodated with penalty terms (ρ^V & ρ^L) multiplied by a penalty weight ($C^\perp$) in the objective function, shown in Eqs. (26), (27) and (112) (case study).

$$0 \leq F_s \perp \sigma_s \geq 0 \qquad \forall s \in \{FlashVap \cup FlashLiq\} \tag{25}$$

$$\rho^V = \sum_{s\in\{FlashVap\}} F_s\sigma_s^V \tag{26}$$

$$\rho^L = \sum_{s\in\{FlashLiq\}} F_s\sigma_s^L \tag{27}$$

The phase disappearance concept has also been extended to the simple thermodynamics module (Eqs. (28) and (29)). The phase(s) of a given stream s are determined by examining bubble and dew point pressures (P^b and P^d, respectively) relative to the stream's overall pressure (P).

$$P_s \geq P_s^b(x_s) - M\sigma_s^L \qquad s \in \{FlashLiq\} \tag{28}$$

$$P_s \leq P_s^d(y_s) + M\sigma_s^V \qquad s \in \{FlashVap\} \tag{29}$$

2.6. Phase verification

It is well established that cubic equations of state can predict spurious (i.e. incorrect) phase compositions under certain conditions, such as $K=1$ (Gundersen, 1982). This is particularly problematic when only a single phase exists. We safeguard against these incorrect phase predictions in the optimization framework by using bubble and dew point temperature calculations in two places. First, Eqs. (30) and (31) are written for streams known *a priori* to be single phase (e.g. the exit of a total condenser is only a liquid). This is required, as Eqs. (20) and (22) are necessary but not sufficient to define a single phase stream. Second, bubble and dew point temperatures are checked for all streams with a non-zero flowrate in a post-processing step.

$$T_s^{bubble} \geq T_s, \qquad \forall s \in \{\text{Select Liquid Streams}\} \tag{30}$$

$$T_s^{dew} \leq T_s, \quad \forall s \in \{\text{Select Vapor Streams}\} \tag{31}$$

3. General unit operation equipment models

Many basic units share a similar structure, as shown in Fig. 1, with one or more input streams and two possible outlet streams (vapor and liquid). These units also share several equations, namely mass and enthalpy balances, and phase equilibria expressions for the outlet streams. Under the theme of modularity flash separators, heat exchangers, partial reboilers, throttle valves and total condensers are classified as "general equipment" and inherit

these common equations. All general equipment except total condensers are also classified as "thermodynamic equipment". General and thermodynamic equipment are represented by $\{GnrlE\}$ and $\{ThrmE\}$ sets, respectively, and $\{ThrmE\} \subset \{GnrlE\}$. For ThrmE units the outlet streams are in thermodynamic equilibrium. Additional pressure and/or temperature relationships are also specified for each type of equipment.

Flowsheet connectivity is managed using compound sets in GAMS. For example $\{InGnrlE\}$ contains pairings of streams (index s) and general equipment (index g). If the pair s^1, g^1 belongs to $\{InGnrlE\}$, it would imply s^1 is an inlet stream for equipment g^1. $\{OutLGnrlE\}$ and $\{OutVGnrlE\}$ establish the outlet liquid and vapor streams for all general equipment. These and similar sets are used to define flowsheet connectivity.

The general equipment model consists of an overall enthalpy balance (Eq. (32)), bounds on heat duty (Eq. (33)), and component mole balances (Eq. (34)). The thermodynamic equipment model also includes equilibrium expressions (Eqs. (35)–(37)). $x_{s^l,c}$ $(y_{s^v,c})$ corresponds to the mole fraction of component c in liquid (vapor) stream s^l (s^v). Eqs. (4) and (25) are rewritten below (without numbers) for clarity.

$$g \in \{GnrlE\}$$
$$s^f \in \{InGnrlE\}(g)$$
$$s^l \in \{OutLGnrlE\}(g)$$
$$s^v \in \{OutVGnrlE\}(g)$$

Overall Enthalpy Balance

$$\forall g, \quad \sum_{sf} F_{sf} H_{sf,c} + Q_g^{in} = F_{sl} H_{sl} + F_{sv} H_{sv} + Q_g^{out} \tag{32}$$

$$Q_g^{in}, Q_g^{out} \geq 0 \tag{33}$$

Component Mole Balance

$$\forall g, c \quad \sum_{sf} f_{sf,c} = f_{sl,c} + f_{sv,c} \tag{34}$$

Thermodynamic Equilibrium

$$\forall g^* \in \{ThrmE\}$$
$$\sum_c x_{sl,c} = 1$$
$$\sum_c y_{sv,c} = 1$$

$$y_{sv,c} = \beta_{g^*} K_{g^*,c} x_{sl,c} \tag{35}$$
$$T_{sv} = T_{sl} \tag{36}$$
$$P_{sv} = P_{sl} \tag{37}$$

$$0 \leq \sigma_{sl}^L \perp F_{sl} \geq 0$$
$$0 \leq \sigma_{sv}^V \perp F_{sv} \geq 0$$

3.1. Flash separation and throttle valves

The flash unit is the simplest type of thermodynamic equipment. Eq. (38) sets P_{flsh} equal to the outlet pressure. Eq. (39) ensures the inlet pressure for each feed stream is no less than P_{flsh}. Finally Eq. (40) restricts flash vessels to adiabatic operation. Recall the flash model also inherits all of the general thermodynamic equipment equations (Eqs. (32)–(37)). Adiabatic throttle valves are mathematically equivalent to flash vessels with these models.

$$P_{sv} = P_{flsh} \tag{38}$$
$$P_{sf} \geq P_{flsh} \tag{39}$$
$$Q_{flsh}^{in} = Q_{flsh}^{out} = 0 \tag{40}$$

3.2. Reboilers, condensers and heat exchangers

Partial reboilers, partial condensers and the fluid (*i.e.* non-utility) side of heat exchangers are non-adiabatic extensions of the flash model. Heat exchangers are further classified as cooling (removing heat, index cgu) or heating (providing heat, index hgu). Partial reboilers are mathematically identical to heating heat exchangers. In addition to the general equipment equations (Eqs. (32)–(37)), the heat exchanger model includes Eq. (41) to relate pressures (recall $P_{sl} = P_{sv}$ per Eq. (37)) and Eqs. (42)–(44) to ensure only heat removal or addition in the applicable units. Flowrates and inlet/outlet temperatures for the utility side of the heat exchangers are not explicitly considered in this model. Instead heat addition (Q^{in}) and removal (Q^{out}) are calculated for each unit.

$$P_{sf} = P_{sl} \tag{41}$$
$$T_{cgu}^{in} \geq T_{cgu}^{out} \tag{42}$$
$$T_{hgu}^{in} \leq T_{hgu}^{out} \tag{43}$$
$$Q_{cgu}^{in} = Q_{hgu}^{out} = 0 \tag{44}$$

3.3. Total condensers and total heat reboilers

Total condensers (and total reboilers) do not have a vapor outlet (liquid for reboiler) stream and thus are not classified as thermodynamic equipment. The mathematical model for these general equipment units includes only mass and enthalpy balances (no phase equilibrium), along with a pressure relationship. In this study condensers are total and reboilers are partial.

4. Distillation models

Optimization of complex distillation systems was pioneered by Sargent and Gaminibandara (1976) and continues to remain a challenging design paradigm. Andrecovich and Westerberg (1985) developed a mixed integer linear programming (MILP) formulation to optimize heat integrated distillation sequences using approximate models. Several assumptions (constant split fractions calculated *a priori*, column fixed costs that only vary with condenser pressure, etc.) are made to avoid nonlinearities. Viswanathan and Grossmann (1990) developed a rigorous mixed integer nonlinear programming (MINLP) model for distillation column optimization. Integer variables are used to select the optimal feed tray location and activate/deactivate trays. The model has been extended to consider a variable number of trays and multiple feeds (Viswanathan and Grossmann, 1993a; Viswanathan and Grossmann, 1993b). The model was also reformulated using disjunctive programming methods (Yeomans and Grossmann, 2000a, Yeomans and Grossmann, 2000b).

Recent work has focused on reformulation of the MINLP distillation column model to remove the integer variables. Embedding the full MINLP column model into a flowsheet with many other nonlinear reactors and separation units may lead to intractable optimization problems. Also, rigorous thermodynamics models add significant nonlinearity and nonconvex constraints to the distillation optimization problem, thus complicating the solution of the

original MINLP problem. By formulating the optimization problem as a pure NLP, the combinatorial nature of the mixed integer problem can be mitigated. This motivated Kamath et al. (2010) to propose a revised shortcut model as an approximate distillation model. Unfortunately there can be significant mismatch between this model and more rigorous mass, equilibrium, summation and heat (MESH) equations for certain distillation systems. Kraemer et al. (2009) investigated relaxations of the integer variables to continuous and inclusion of a nonlinear Fischer–Burmeister function constraint to drive these variables to 0 or 1 values. The approach has some drawbacks; most notably the interior of relaxed integer variables (non-binary values) are ill-defined, leading to local solutions and even infeasibilities when the problem is not carefully initialized. This key downside has motivated development of a new MESH model with bypass that has physically realizable relaxations.

The remainder of this section is organized as follows: a general cascade structure is introduced, which is used for both distillation column models. Next the shortcut model studied by Kamath et al. (2010) is summarized. Finally a new rigorous tray-by-tray model is presented.

4.1. General cascade structure and feed location

Cascade sections are linked together to form distillation, absorption and stripping columns with flash vessels used for feed trays. A general superstructure is shown in Fig. 2. The feed stream (*S0*) is split into S1, S2 and S3 via splitter 1. These streams act as feeds for flash vessels *F1*, *F2* and *F3*, which correspond to the bottom, a middle and the top trays in the column. Cascade sections (whose models are discussed in this section) are located between the flash vessels. This superstructure allows for selection of an absorption, stripping or distillation column, along with hybrid configurations. Also shown in Fig. 2 are the four main streams for each cascade section: inlet vapor (*S6*, *S12*), inlet liquid (*S4*, *S14*), outlet vapor (*S5*, *S13*) and outlet liquid (*S7*, *S11*).

4.2. Edmister approximation

A modified Edmister approximation (Kamath et al., 2010) is used to model distillation cascades with a continuous number of equilibrium stages (N^{stg}) and no integer variables. At the heart of the model are component mole balances (Eq. (45)), an enthalpy balance (Eq. (46)) and performance equation (Eq. (47)). The recovery factors for absorption (φ^A) and stripping (φ^S) are used in the performance equations and are calculated from Eqs. (49) and (50). These equations are log transformations of the original model in Kamath et al. (2010) and include two intermediate variables (I^A & I^S). Based on empirical observations, this reformulation provides better scaled derivatives and improved numeric performance. The absorption factors are calculated from equilibrium expressions at the column outlets, which require separate implementations for each thermodynamics module (Eqs. (58) and (59) for the simple thermo. module, Eqs. (62) and (63) for CEOS). The stripping factors are related to the absorption factors, as shown in Eqs. (55) and (56). These factors are averaged using the original formula proposed by Edmister (Eqs. (53) and (54)).

This model contains two modifications proposed by Kamath et al. (2010). The first modification is an approximate mole balance, shown in Eq. (48). This replaces the absorber and stripping specific equations proposed by Edmister (1957), making the model general to either stripping or absorbing cascades. In the second modification the temperature approximations are replaced by bubble and dew point calculations for the outlet liquid and vapor streams, respectively. This requires separate implementations for each thermodynamic module. Calculation of the bubble and dew point is already part of the simple thermodynamics model, making Eqs. (60) and (61) straightforward. Bubble and dew point constraints with the cubic EOS thermodynamics model requires the introduction of shadow streams (s^{v*}, s^{l*}) that are in equilibrium with the outlet streams (Eqs. (64) and (65)). The shadow streams are also used to calculate the adsorption factors, as shown in Eqs. (62) and (63). Consistent with the general equipment models, compound sets are used to represent connectivity for the distillation cascades. The sets {*InVEd*}, {*InLEd*}, {*OutVEd*} and {*OutLEd*} map inlet-vapor, inlet-liquid, outlet-vapor and outlet-liquid streams *s* with each cascade *ed*.

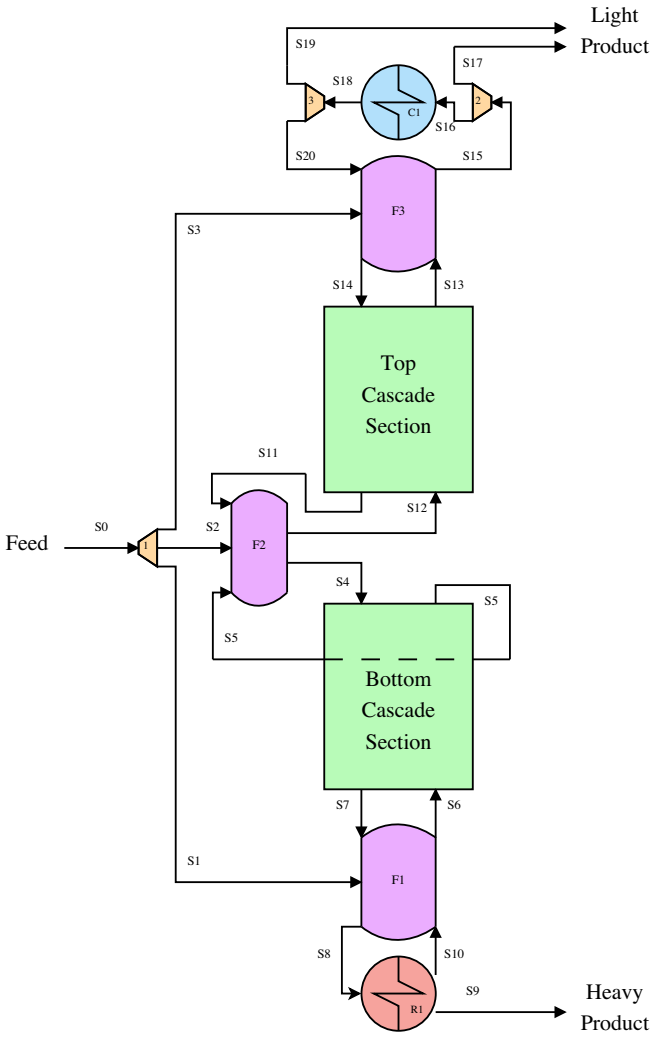

Fig. 2. Distillation column structure with variable feed location.

Distillation Cascade Model

$ed \in \{\text{Cascades}\}$

$s^{iv} \in \{InVEd\}(ed)$

$s^{il} \in \{InLEd\}(ed)$

$s^{ov} \in \{OutVEd\}(ed)$

$s^{ol} \in \{OutLEd\}(ed)$

$$f_{s^{il}} + f_{s^{iv}} = f_{s^{ov}} + f_{s^{ol}} \tag{45}$$

$$F_{s^{il}} H_{s^{il}} + F_{s^{iv}} H_{s^{iv}} = F_{s^{ov}} H_{s^{ov}} + F_{s^{ol}} H_{s^{ol}} \tag{46}$$

$$f_{s^{ov},c} = f_{s^{iv},c}\varphi^{A}_{ed,c} + f_{s^{il},c}(1-\varphi^{S}_{ed,c}) \tag{47}$$

$$L^{1}_{ed} - F_{s^{ol}} = F_{s^{ov}} - V^{N}_{ed} \tag{48}$$

$$(N^{stg}_{ed}+1)\ln(A^{e}_{ed,c}) = \ln(I^{A}_{ed,c}) - \ln(\varphi^{Ae}_{ed,c}) \tag{49}$$

$$(N^{stg}_{ed}+1)\ln(S^{e}_{ed,c}) = \ln(I^{S}_{ed,c}) - \ln(\varphi^{Se}_{ed,c}) \tag{50}$$

$$I^{A}_{ed,c} = A^{e}_{ed,c} - 1 + \varphi^{Ae}_{ed,c} \tag{51}$$

$$I^{S}_{ed,c} = S^{e}_{ed,c} - 1 + \varphi^{Se}_{ed,c} \tag{52}$$

$$A^{e}_{ed,c} = \sqrt{A^{N}_{ed,c}\left(A^{1}_{ed,c}+0.25\right)} - 0.5 \tag{53}$$

$$S^{e}_{ed,c} = \sqrt{S^{1}_{ed,c}\left(S^{N}_{ed,c}+0.25\right)} - 0.5 \tag{54}$$

$$S^{1}_{ed,c}A^{1}_{ed,c} = 1 \tag{55}$$

$$S^{N}_{ed,c}A^{N}_{ed,c} = 1 \tag{56}$$

$$P_{ed} = P_{s}, \quad s \in \{OutLEd \cup OutVEd \cup InVEd \cup InLEd\}(ed) \tag{57}$$

Simple Thermo Module

$$A^{1}_{ed,c}F_{s^{ov}}P^{vap}_{s^{ov},c} = L^{1}_{ed}P_{ed} \tag{58}$$

$$A^{N}_{ed,c}V^{N}_{ed}P^{vap}_{s^{ol},c} = F_{s^{ol}}P_{ed} \tag{59}$$

$$P_{s^{ov}} = P^{d}_{s^{ov}} \tag{60}$$

$$P_{s^{ol}} = P^{b}_{s^{ol}} \tag{61}$$

CEOS Thermo Module

$$A^{1}_{ed,c} \quad F_{s^{ov}} \quad \phi_{s^{l*},c} = L^{1}_{ed}\phi_{s^{ov},c}$$
$$s^{ov}, s^{l*} \in \{DPStr\} \tag{62}$$

$$A^{N}_{ed,c} \quad V^{N}_{ed} \quad \phi_{s^{ol},c} = F_{s^{ol}} \quad \phi_{s^{v*},c}$$
$$s^{ol}, s^{v*} \in \{BPStr\} \tag{63}$$

$$T^{*}_{s^{ov}} = T^{*}_{s^{l*}}, \quad P_{s^{ov}} = P_{s^{l*}} \tag{64}$$

$$T^{*}_{s^{ol}} = T^{*}_{s^{v*}}, \quad P_{s^{ol}} = P_{s^{v*}} \tag{65}$$

4.3. Tray-by-tray model with bypass

Kremser's shortcut model assumes the separation factor remains constant in the cascade (see Biegler et al. (1997) for a derivation); in real cascades this can lead to approximation error. For these systems rigorous mass, equilibrium, summation and heat (MESH) models for each discrete tray should be considered. This requires the number of discrete trays to be fixed *a priori* or represented by integer variables, such as in Viswanathan and Grossmann (1990). The model for each tray is straightforward, consisting of component mole balances (Eq. (66)), equilibrium calculations (Eqs. (68)–(71)), and an enthalpy balance (Eq. (67)). The summation equations are part of the stream model (Eq. (4)). Pressure drop is also included in the tray model (Eqs. (72) and (73)), where ΔP_{ed} represents the pressure drop per tray coefficient. N^{stg}_{ed} represents the number of trays per cascade which is initially fixed. In this framework the MESH cascade model is only implemented with the cubic EOS thermodynamics module.

Compound sets are also used to manage tray connectivity. {*TraysCascs*} maps trays n to each cascade ed. Similarly {*InTrL*}, {*InTrV*}, {*OutTrL*} and {*OutTrV*} map inlet/outlet, vapor/liquid streams s to trays n. For the MESH equations below both the tray inlet/outlet streams (s^{in}, s^{out}, s^{ovt} and s^{olt}) and cascade inlet/outlet streams (s^{il}, s^{ol}, s^{iv}, and s^{ov}) are used.

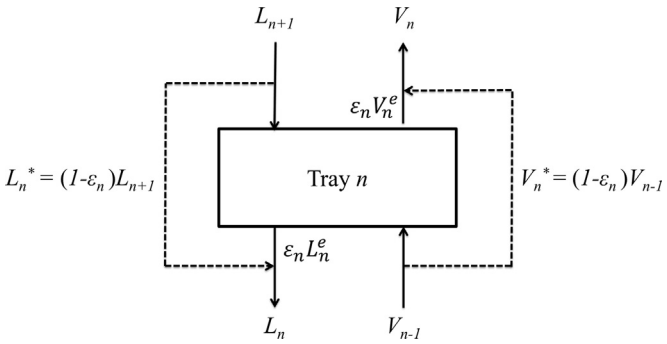

Fig. 3. Single tray with bypass streams.

$$n \in \{TraysCasc\}(ed)$$
$$s^{in} \in \{InTrL \cup OutTrV\}(n)$$
$$s^{out} \in \{OutTrL \cup OutTrV\}(n)$$
$$s^{ovt} \in \{OutTrV\}(n)$$
$$s^{olt} \in \{OutTrL\}(n)$$
$$s^{iv} \in \{InVEd\}(ed)$$
$$s^{il} \in \{InLEd\}(ed)$$
$$s^{ov} \in \{OutVEd\}(ed)$$
$$s^{ol} \in \{OutLEd\}(ed)$$

$$\sum_{s^{in}} F^{c}_{s^{in},c} = \sum_{s^{out}} F^{c}_{s^{out},c} \qquad \forall c \in \{Comps\} \tag{66}$$

$$\sum_{s^{in}} F_{s^{in}} H_{s^{in}} = \sum_{s^{out}} F_{s^{out}} H_{s^{out}} \tag{67}$$

$$K_{tr,c}\phi_{s^{ovt},c} = \phi_{s^{olt},c} \qquad \forall c \in \{Comps\} \tag{68}$$

$$y_{s^{ovt},c} = K_{tr,c}x_{s^{olt},c} \quad \forall c \in \{Comps\} \tag{69}$$

$$T_{s^{olt}} = T_{s^{ovt}} \tag{70}$$

$$P_{s^{ovt}} = P_{s^{olt}} \tag{71}$$

$$P_{s^{vi}} = P_{s^{li}} + (N^{stg}_{ed})(\Delta P_{ed}) \tag{72}$$

$$P_{s^{ovt}} = P_{s^{ivt}} - \Delta P_{ed} \tag{73}$$

We extend the standard MESH model by considering bypass streams for each tray, as shown in Fig. 3. The liquid and vapor flows into tray n, L_{n+1} and V_{n-1}, respectively, are split creating the bypass streams L^{*}_{i} and V^{*}_{n}. The non-bypassed remainder of the vapor and liquid flows enter tray n. If no bypass occurs (flows in L^{*}_{n} and V^{*}_{n} are zero), the standard MESH model is obtained and the outlet streams (L_n and V_n) are in vapor–liquid equilibrium. In contrast, with total bypass no separation is achieved and the inlet streams are identical to the outlets. As a result partially bypassed trays are well defined and the feasible region is not disjoint.

$$\varepsilon_n = 1 - \frac{V^{*}_{n}}{V_{n-1}} = 1 - \frac{L^{*}_{n}}{L_{n+1}} \tag{74}$$

$$\text{Number of Trays } (N^{stg}_{ed}) \approx \sum_{n} \varepsilon_n \tag{75}$$

Let the ratio of non-bypassed flow to total flow into the tray section be defined as the bypass efficiency (ε_n), as shown in

Eq. (74). The number of trays in each cascade is computed by summing the tray efficiencies, shown in Eq. (75).

The MESH distillation model with bypass is solved as a sequence of NLPs and initialization steps, described below and illustrated in Fig. 4:

1. First, the entire flowsheet is optimized and the shortcut cascade model is used for any distillation units. If the optimized flowsheet includes any non-integer number of trays, these values are rounded and fixed, and the entire flowsheet is then reoptimized. This provides a flowsheet solution with an integer number of trays that is used to initialize the MESH model.
2. Next, the MESH model with tray bypass is initialized using the same number of active (non-bypassed) trays as the previous solution. A specified number of additional trays (e.g. ten) are also included in the distillation superstructure. These trays are initialized as inactive (bypassed). This permits the optimizer to turn on additional trays and expand the cascade, similar to the approach from Viswanathan and Grossmann (1990), thus making the number of trays an optimized variable.
3. After initialization the flowsheet is optimized using the MESH model with bypass for all distillation units.
4. Next the solution is analyzed and additional trays are added or removed in order to reinitialize a fixed number of inactive trays (e.g. ten).
5. The flowsheet is then reoptimized and the process either terminates or repeats by returning to step 4. Potential termination criteria include the following: (1) stop if there is no change in the number of trays from the previous iteration; (2) stop if there is at least one completely inactive tray for each cascade or the maximum number of trays are allocated for each cascade; or (3) stop after a fixed number of iterations. Detailed analysis of the proposed termination criterion is left as future work. In this case study we found terminating after three cycles is sufficient and the simplest to implement.

Experience with the ASU case study has shown using ten to twenty initially inactive trays balances the ability of cascades to grow with computational complexity. If too many initially inactive trays are used the full flowsheet NLP will require noticeably more time to solve. In some cases, CONOPT was observed to terminate at infeasible points with 50+ initially inactive trays for the ASU case study. (The ideal number of initially inactive trays is likely different for other distillation systems and flowsheets. We also found the number of initially inactive trays can impact the local solution found when solving the model. For this reason the number of initially inactive trays is considered in the multi-start procedure described in Section 6.)

With total bypass there is no feed flow ($V_{n-1} - V_n^* = 0$ and $L_{n+1} - L_n^* = 0$) and the equilibrium equations in the MESH model are degenerate. To avoid this problem, the bypass equations are reformulated such that equilibrium is calculated with L_{n+1} and V_{n-1}. The bypass fraction is applied for the mass and enthalpy balances around mixers. Let L_n^e and V_n^e represent the total flowrate for hypothetical streams exiting tray n without bypass (as with the standard MESH equation model). Also let $l_{n,c}, l_{n,c}^*, l_{n+1,c}, l_{n,c}^e, v_{n,c}, v_{n,c}^*, v_{n-1,c}, v_{n,c}^e$ represent the flowrate of component c in streams with total molar flowrates L_n, $L_n^*, L_{n+1}, L_n^e, V_n, V_n^*, V_{n-1}$ and V_n^e, respectively. All of these streams, except L_n^e and V_n^e (which are hypothetical), are shown in Fig. 3. With these definitions the following relationships hold:

$$l_{n,c} = x_{n,c} \quad L_n$$

$$v_{n,c} = y_{n,c} \quad V_n$$

First consider equilibrium calculations to determine the flows and composition of L_n^e and V_n^e. Recall these stream properties are calculated without bypass, ensuring flowrates used for the equilibrium calculations are non-zero. L_{n+1} and V_{n-1} are bounded away from zero, preventing vanishing phases at the final solution. β_n is included in Eq. (78) to assist with convergence.

$$v_{n-1,c} + l_{i+1,c} = v_{n,c}^e + l_{n,c}^e, \quad \forall c \in \{Comps\} \tag{76}$$

$$V_{n-1}H^{V_{n-1}} + L_{n+1}H^{L_{n+1}} = V_n^e H^{V_n^e} + L_n^e H_n^{L^e} \tag{77}$$

$$y_c^{V_n^e} = \beta_n K_{n,c} x_c^{L_n^e}, \quad \forall c \in \{Comps\} \tag{78}$$

$$T^{V_n^e} = T^{L_n^e} \tag{79}$$

$$K_{n,c}\phi_c^{V_n^e} = \phi_c^{L_n^e}, \quad \forall c \in \{\text{Comps}\} \tag{80}$$

Next, consider mass and enthalpy balances for two mixers that combine the bypass and streams in equilibrium. These equations are used to calculate the composition and temperature of streams L_n and V_n. Note the definition of ε_n (Eq. (74)) is used to implicitly calculate flowrates for bypass streams (L_n^* and V_n^*).

$$v_{i,c} = \varepsilon_n v_{n,c}^e + (1-\varepsilon_n)v_{n-1,c} \tag{81}$$

$$l_{i,c} = \varepsilon_n l_{n,c}^e + (1-\varepsilon_n)l_{n+1,c} \tag{82}$$

$$L_n H^{L_n} = \varepsilon_n H^{L_n^e} L_n^e + (1-\varepsilon_n)L_{n+1}H^{L_{n+1}} \tag{83}$$

$$V_n H_n^V = \varepsilon_i H^{V_n^e} V_n^e + (1-\varepsilon_n)V_{n-1}H^{V_{n-1}} \tag{84}$$

$$0 \le \varepsilon_n \le 1 \tag{85}$$

Finally the pressure drop relations are specified. Similar to Eq. (38), the cascade outlet streams are in pressure equilibrium (Eq. (86)). The hypothetical equilibrium stream pressures also match the outlet streams (Eqs. (87) and (88)). The ability to activate and deactivate trays is retained by modeling the pressure drop on each tray as proportional to the bypass fraction (Eq. (89)). Eq. (72) is retained to relate the top and bottom pressures in the entire cascade.

$$P^{L_n} = P^{V_n} \tag{86}$$

$$P^{L_n} = P^{L_n^e} \tag{87}$$

$$P^{V_n} = P^{V_n^e} \tag{88}$$

$$P^{V_n} = P^{V_{n-1}} - \varepsilon_n \Delta P_{ed} \tag{89}$$

5. Heat integration models

Heat integration is an essential strategy for reducing costs in a chemical or power generation plant. The overall goal is to reduce the use of hot and cold utilities by reusing waste heat and cooling available throughout the process. From an optimization perspective, the problem can be formulated as follows: *Given heating and cooling demands in a process, minimize the total cost (equipment, utilities) for heat exchange subject to the laws of thermodynamics.* This problem, known as *heat exchanger network synthesis* (HENS), is addressed by two general methods: (1) graphical pinch and (2) mathematical programming. See Linnhoff (1993) and Furman and Sahinidis (2002), respectively, for comprehensive reviews of these methods.

Both graphical pinch and mathematical programming methods for heat integration assume fixed process stream cooling and heating demands. For many process design applications, such as optimization of heat integrated distillation columns, simultaneous flowsheet optimization (adjust flowrates, temperatures, pressures, etc.) and heat integration leads to more cost effective designs due to the additional degrees of freedom. To accommodate these interactions, Duran and Grossmann (1986) developed a formulation

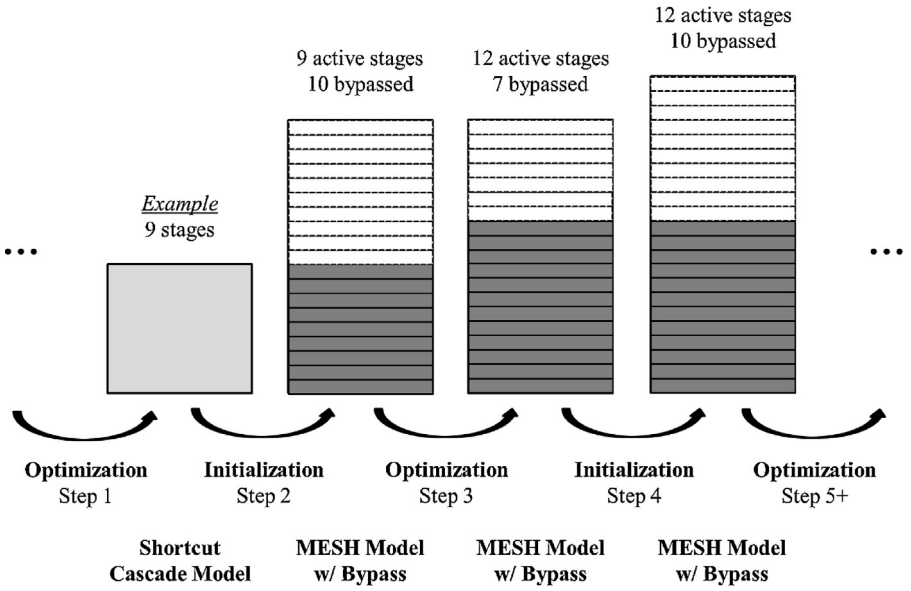

Fig. 4. Distillation initialization schematic. Dark trays are active and light trays are bypassed. During the initialization step the cascade model is resized such that there are ten initially bypassed trays.

where pinch equations are embedded in a flowsheet optimization problem. Although this approach allows for the simultaneous calculation of minimum utilities and adjustment of flowsheet operating conditions, it does not consider heat exchanger matches. It has been successfully demonstrated on several applications, including optimization of the PRICO process for natural gas liquefaction by Kamath et al. (2012). The Duran–Grossmann approach is included in this framework for flowsheet optimization with modifications. Here we first introduce general naming conventions within the Duran–Grossmann formulation. This includes an extension with multiple heat integration zones. Next a modification to reduce errors from the smoothed max operator is presented. Finally we discuss a method for refining the pinch location results to ensure accurate solutions with nonlinear heat capacities.

5.1. Generalized heat integration units

Reboilers, condensers and heat exchangers are considered for heat integration in this framework. As discussed in Section 3, these units are abstracted as general equipment (*GnrlE*), leading to a compact heat integration model. These equipment are further classified as heating units that require external heating (*e.g.* reboilers) or cooling units that require external cooling (*e.g.* condensers). The indices *hgu* and *cgu* refer to heating and cooling general units, respectively.

This definition is in contrast to the heat integration literature, where the primary goal is to synthesize a heat exchange network with fixed inlet/out stream data (temperatures, flows, etc). In this approach a different problem is addressed: optimize a flowsheet while creating a heat integration network that requires minimum utilities (*i.e.* embed energy targeting into the flowsheet problem).

5.2. Duran and Grossmann model

The Duran and Grossmann model allows for simultaneous flowsheet optimization and heat integration, and is analogous to the transshipment model. The complementarities for the KKT conditions are accommodated with the smoothed max operator (Dowling and Biegler, 2013). In the first section of the model (Eqs. (90)–(93)), temperatures from the streams are copied into variables indexed over the units considered for heat integration. A smoothed max operator (Eq. (106)) is used in conjunction with a small number (α) to ensure nonzero temperature drops for phase changes. For a high purity stream undergoing phase change (*e.g.* boiling) the temperature change is near zero and the calculated heat capacity is nearly infinite, resulting in numerical difficulties. In Duran and Grossmann (1986) $\alpha = 1$ K is considered in Eqs. (91) and (92). For cryogenic applications with a small minimum driving force (<2 K) a smaller α (0.1–0.2 K) is used.

In the second section, Eqs. (94)–(97), the inlet and outlet temperatures for each heat exchange unit are considered as pinch candidates. The minimum driving force temperature constant (ΔT^{min}) is added to the inlet and outlet temperatures of heating units (*e.g.* reboilers), which correspond to cold streams in Duran and Grossmann (1986), Linnhoff (1993). For flowsheet design problems, extreme stream temperatures are generally not known *a priori*; thus all of the inlet and outlet streams are considered as pinch candidates in this framework. Although this increases problem size, it has little impact on the results. In the third section, Eqs. (98)–(99), the average heat capacity-flowrate term (FCp_{gu}) for each unit is calculated. The formulation assumes that the heat capacity for each stream is constant over the temperature interval considered.

The heart of the model is contained in the final two sections. The heating and cooling available above each pinch candidate is calculated using Eqs. (102) and (103), respectively. The maximum utility usage occurs at a pinch point, thus Eq. (104) is used to calculate the minimum hot utility requirement $\overline{Q}^s$. The minimum cold utility requirement is calculated using an enthalpy balance, as shown in Eq. (105).

$$T^{in}_{hgu} = T_{sf,hx} \tag{90}$$

$$T^{out}_{hgu} = \tilde{\max}(T_{sv,hgu} - T_{sf,hx} - \alpha, 0) + T_{sf,hx} + \alpha \tag{91}$$

$$T^{in}_{cgu} = \tilde{\max}(T_{sf,hx} - T_{sv,cgu} - \alpha, 0) + T_{sv,cgu} + \alpha \tag{92}$$

$$T^{out} = T_{sv,cgu}, \quad z \in \{HIZones\} \tag{93}$$

$$TP_{sf,cgu,z} = T^{in}_{cgu(z)} \tag{94}$$

$$TP_{sl,cgu,z} = T^{out}_{cgu(z)} \tag{95}$$

$$TP_{sf,hgu,z} = T^{in}_{hgu(z)} + \Delta T^{\min}_{z} \tag{96}$$

$$TP_{s^{l,hgu},z} = T^{out}_{hgu(z)} + \Delta T^{\min}_z \tag{97}$$

$$Q^{in}_{hgu} = FCp_{hgu}(T^{out}_{hgu} - T^{in}_{hgu}) \tag{98}$$

$$Q^{out}_{cgu} = FCp_{cgu}(T^{in}_{cgu} - T^{out}_{cgu}) \tag{99}$$

$$\Delta T^{\max} \geq T_{s^{v,cnd}} - T_{s^{l,v}} \tag{100}$$

$$\Delta T^{\max} \geq T_{s^{v,reb}} - T_{s^{f,reb}} \tag{101}$$

$$Q^{Ah}_{s^P,z} = \sum_{cgu(z)} FCp_{cgu}[\tilde{\max}(T^{in}_{cgu} - TP_{s^P}, 0) - \tilde{\max}(T^{out}_{cgu} - TP_{s^P}, 0)] \quad \forall s^P \in \{\text{Pinch Candidates}(z)\} \tag{102}$$

$$Q^{Ac}_{s^P,z} = \sum_{hgu(z)} FCp_{hgu}[\tilde{\max}(T^{out}_{hgu} - TP_{s^P} + \Delta T^{\min}_z, 0) - \tilde{\max}(T^{in}_{hgu} - TP_{s^P} + \Delta T^{\min}_z, 0)] \quad \forall s^P \in \{\text{Pinch Candidates}(z)\} \tag{103}$$

$$\bar{Q}^s_z \geq Q^{Ac}_{s^P,z} - Q^{Ah}_{s^P,z} \tag{104}$$

$$\bar{Q}^w_z = Q^s_z + \sum_{gu(z)} \left[Q^{out}_{gu} - Q^{in}_{gu}\right] \tag{105}$$

$$s^{f,gu} \in \{InGnrlEOne\}$$

$$s^{v,hgu} \in \{OutVGnrlE\} \cap \{HeatGnrlE\}$$

$$s^{v,cgu} \in \{OutVGnrlE\} \cap \{CoolGnrlE\}$$

$$\tilde{\max}(x, 0) = \frac{1}{2}[x + \sqrt{x^2 + \epsilon^2}] \approx \max(x, 0) \tag{106}$$

The Duran–Grossmann formulation is extended by considering multiple heat exchanger zones, which allows for different groups of process units to be heat integrated separately. For example, in a cryogenic air separation unit the multistream heat exchanger streams would be assigned to one zone, whereas the coupled reboiler/condenser would be assigned to another. Furthermore, each zone may have a different ΔT^{min} value. Many of the above equations are indexed over z, denoting the equations that are replicated for each zone. The minimum utility demands for the overall process (Q^s, Q^w) are calculated using Eqs. (107) and (108).

$$Q^s = \sum_{z \in \{HIZones\}} \bar{Q}^s_z \tag{107}$$

$$Q^w = \sum_{z \in \{HIZones\}} \bar{Q}^w_z \tag{108}$$

5.3. Reformulation to reduce smoothed max errors

The smoothed max operator (Eq. (106)) blends the kink at the switching point ensuring differentiability for gradient based optimization. However this adds small numerical errors, especially near the switching point/kink. Near the switching point at $x = 0$, $\tilde{\max}(0, 0)$ returns 0.5ϵ, whereas $\max(0, 0) = 0$. The smoothed max operator also contributes to large elements of $O(1/\epsilon)$ in the Hessian near the switching point, which may lead to poor optimizer performance. Most evaluations of $\tilde{\max}()$ near the switching point are inside the summations of Eqs. (102) and (103) and occur when the inlet or outlet streams correspond to the pinch candidate stream (s^P). These cases can be removed by analyzing each $\tilde{\max}$ term and unrolling the summations in Eqs. (102) and (103). The zone index z is omitted in this section for brevity.

Table 2
Heat available for integration at switching points.

	Heating unit ($T^{in} \leq T^{out}$)	Cooling unit ($T^{in} \geq T^{out}$)
$T^{in}_{cgu} = TP_{s^P}$	0	Q^{out}_{cgu}
$T^{out}_{hgu} = TP_{s^P}$	Q^{in}_{hgu}	0

To illustrate this idea, consider the heat available for integration of a specific heating unit (index hgu) as a function of pinch temperature (TP), as shown in Fig. 5. When the pinch temperature is less then the inlet temperature for the unit (T^{in}_{hgu}), no heat is available from the unit for heat integration (vertical axis). Likewise for pinch candidate temperatures above the outlet temperature (T^{out}_{hgu}), the total heat load for the unit (Q^{in}_{hgu}) is available for heat integration. If the pinch temperature is between the inlet and outlet temperature, linear interpolation is used to calculate the heat available for integration (a consequence of the constant heat capacity assumption). This description is consistent with Eq. (103), and thus $TP = T^{in}_{hgu}$ and $TP = T^{out}_{hgu}$ correspond to the switching points of the smoothed max operator Eq. (103). Table 2 summarizes the heat available for integration at all four switching points in Eqs. (102) and (103). The first column of the table corresponds with the scenarios in Fig. 5.

These scenarios provide justification to reformulate Eqs. (102) and (103) to Eqs. (109) and (110). The summations are unrolled and units whose inlet or outlet streams are the pinch candidates are considered separately (without the $\tilde{\max}$ operator). This is best illustrated by considering an example heating unit (hgu^*) and Eq. (103). When the pinch candidate stream (s^P) corresponds with the inlet stream for unit hgu^* the contribution to the summation in Eq. (103) is zero (see Table 2). Likewise when s^P corresponds with the outlet stream the available heat for integration from hgu^* is $Q^{in}_{hgu^*}$. This leads to some set definitions: for a specified s^P let $\{H^1\}$ contain all heating units whose inlet or outlet streams are NOT s^P. Let $\{H^2\}$ contain the units whose outlet stream is s^P and $\{H^3\}$ contain the units whose inlet stream is s^P. Using these sets the summation in Eq. (103) is unrolled and scenarios presented in Table 2 are applied to simplify the summations over $\{H^2\}$ and remove the summation over $\{H^3\}$, ultimately yielding the second line of Eq. (109).

$$\begin{aligned} Q^{Ac}_{s^P} &= \sum_{hgu \in \{H^1\}} FCp_{hgu}[\tilde{\max}(T^{out}_{hgu} - TP_{s^P} + \Delta T^{\min}, 0) - \tilde{\max}(T^{in}_{hgu} - TP_{s^P} + \Delta T^{\min}, 0)] \\ &\quad + \sum_{hgu \in \{H^2\}} FCp_{hgu}[\tilde{\max}(T^{out}_{hgu} - TP_{s^P} + \Delta T^{\min}, 0) - \tilde{\max}(T^{in}_{hgu} - TP_{s^P} + \Delta T^{\min}, 0)] \\ &\quad + \sum_{hgu \in \{H^3\}} FCp_{hgu}[\tilde{\max}(T^{out}_{hgu} - TP_{s^P} + \Delta T^{\min}, 0) - \tilde{\max}(T^{in}_{hgu} - TP_{s^P} + \Delta T^{\min}, 0)] \\ &= \sum_{hgu \in \{H^1\}} FCp_{hgu}[\tilde{\max}(T^{out}_{hgu} - TP_{s^P} + \Delta T^{\min}, 0) - \tilde{\max}(T^{in}_{hgu} - TP_{s^P} + \Delta T^{\min}, 0)] \\ &\quad + \sum_{hgu \in \{H^2\}} Q^{in}_{hgu} + \sum_{hgu \in \{H^3\}} 0 \end{aligned} \tag{109}$$

$$Q^{Ah}_{s^P} = \sum_{cgu \in \{C^1\}} FCp_{cgu}[\tilde{\max}(T^{in}_{cgu} - TP_{s^P}, 0) - \tilde{\max}(T^{out}_{cgu} - TP_{s^P}, 0) + \sum_{cgu \in C^2} Q^{out}_{cgu} \tag{110}$$

The same observations are also applied to the cooling units, as seen in Eq. (110), where $\{C^1\}$ contains units whose inlet or outlet streams are NOT s^P and $\{C^2\}$ contains the units whose inlet stream are s^P.

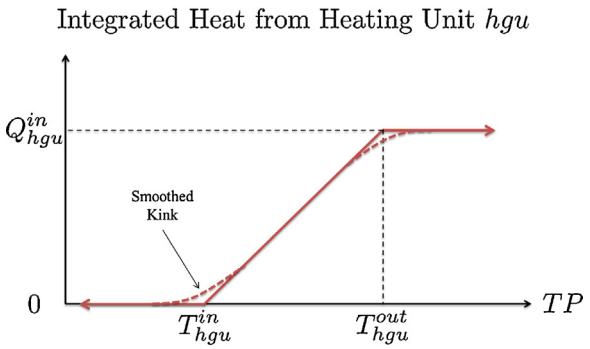

Fig. 5. Cartoon showing the amount of heat integrated in the network for a specific heating unit *hgu* as a function of pinch temperature (*TP*).

5.4. Selection of piecewise constant heat capacities

The pinch based model proposed by Duran and Grossmann (1986) assumes constant heat capacities for each stream. This approximation is typically accurate, except when streams undergo a phase transition. At the bubble and dew point temperatures there is a non-smooth kink in heat capacity. Kamath et al. (2012) propose an extension of the pinch heat integration model that decomposes streams into three substreams (vapor, liquid and two phase) that are separately considered for heat integration.

In this framework, multiple heat exchangers are considered in series for streams undergoing phase changes. For example, in cryogenic systems the feed stream (air) is cooled from a vapor to liquid. Three heat exchangers are used as shown in Fig. 6. The outlet of the first exchanger is constrained to be at the dew point ($\sigma^L = \sigma^V = 0$, $F^L = 0$) and outlet of the second is at the bubble point ($\sigma^L = \sigma^V = 0$, $F^V = 0$). The exit of the final heat exchanger is constrained to be a liquid ($\sigma^V = 0$). Although this approach requires *a priori* specification of streams undergoing multiple phase transitions, it is easier to simulate and verify with commercial flowsheeting tools.

For large changes in temperature heat capacity may not be constant. In order to address this issue, heat exchange units are decomposed into subunits for post-optimization analysis (and possible reoptimization). For example, the three units in series from Fig. 6a are decomposed into two subunits each, as shown in Figs. 6b and 7. The subunits are equally spaced with respect to temperature and maintain the original inlet and outlet conditions of the non-decomposed unit. For heat integrated distillation, this is especially important for condensers and reboilers that may subcool or superheat in addition to change phase. Pinch analysis is then performed after optimization with the subunits, allowing for calculation of a more realistic ΔT^{min} and heat integration curves.

The validation step is formulated as the optimization problem shown below,

$$\min \sum_{s\in\{Str\}} \left[(F_s - \hat{F}_s)^2\right] + \sum_{c}\sum_{s\in\{S^1\}} \left[10(x_{s,c} - \hat{x}_{s,c})^2\right] + 100\rho^L + 100\rho^V$$

s.t. Decomposed Heat Exchanger Connectivity

Stream Models	Eqs. 2 – 4
Thermodynamics Models	Eqs. 6, 15 – 24, 26 – 27, 113 – 121
Heat Exchanger Equipment Models	Eqs. 32 – 37, 41 – 44
Fixed Stream Temperatures	

where $\hat{F}_s$ and $\hat{x}_{s,c}$ correspond to the target stream flowrates and compositions, adopted from the original flowsheet optimization solution. ρ^L and ρ^V are the liquid and vapor complementarity violations, respectively (see Eqs. (26) and (27)). $\{S^1\}$ is the set inlet and outlet streams of the original units (i.e., outermost streams in a series of subunits). The constraints include the decomposed connectivity (e.g. subunits k through $k+n$ are assigned to original unit i) along with the original stream, thermodynamics and heat exchanger equipment models. Finally the temperatures of each stream are fixed.

At the solution the objective function of the heat integration validation problem must be zero, indicating the flowrates and compositions match the specified target values and there are no thermodynamic complementarity violations. Using the inlet and outlet temperatures for each subunit, pinch curves are constructed and a realistic ΔT^{min} is calculated. If the new ΔT^{min} is reasonably close to the old value, the heat integration results have been validated. Otherwise the flowsheet needs to be reoptimized and heat integrated with decomposed general heat exchange units.

6. Practical concerns

Optimization of our non-convex flowsheet models results in numerous local solutions (over 100 observed for the ASU case study). A systematic, reliable initialization procedure helps identify some of the best local solutions. In this paper two complementary strategies are used as the basis of a reliable, systematic initialization procedure. First the flowsheet models are initialized as a sequence of NLPs with increasing model complexity. Second, several parameters (bounds, initial values) were identified as influential to the final results. Combinations of various levels of these parameters are explored in a multi-start procedure to identify multiple local solutions.

6.1. Model refinement for initialization

Model refinement is used to initialize highly nonlinear parts of the flowsheet model, as shown in Fig. 8. The flowsheet is first optimized with simpler, less nonlinear models (cascade approximation, ideal gas/liquid thermodynamics). Model complexity is increased in subsequent NLP problems with

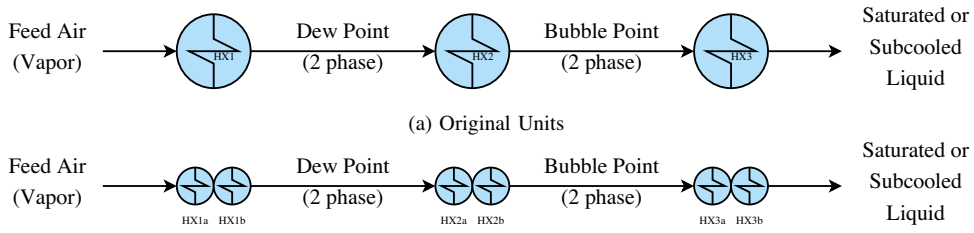

Fig. 6. Cooling heat exchangers in series.

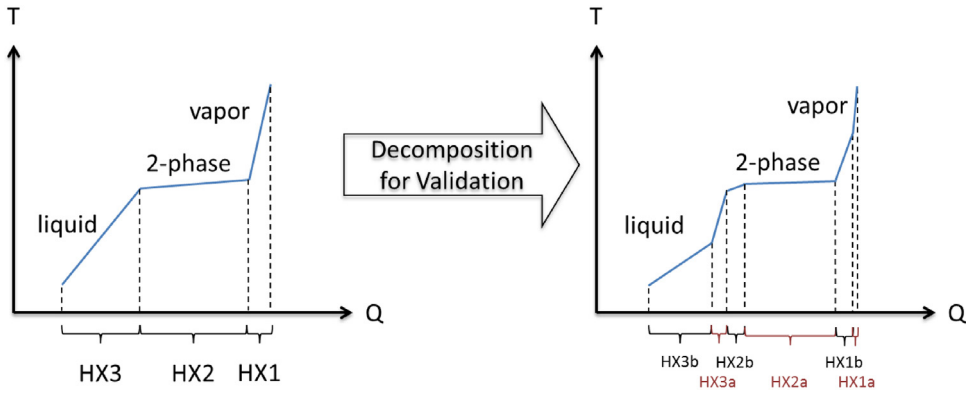

Fig. 7. Decomposition of heat exchanges from Fig. 6 into two subunits each.

the eventual optimization of the flowsheet with CEOS thermodynamics, MESH cascade models and many heat exchange subunits. The six detailed initialization steps used for the framework are described in the supplementary material. Similar model refinement strategies are employed in Kossack et al. (2006).

6.2. Flowsheet pruning to avoid degeneracies

In flowsheet optimization problems, when streams vanish the nonlinear flash equations becomes degenerate, i.e. the Jacobian of the active set is rank deficient. As a result when NLP algorithms calculate a Newton-step, they must invert a singular matrix, resulting in numerical problems. Furthermore, these singularities violate constraint qualifications that provide guarantees about the optimal solution (e.g. unique multipliers). Different algorithms have different safeguards to mitigate this. For example, if the Jacobian is degenerate, CONOPT attempts to determine the offending equations and remove them from the active set. Interior point methods, such as IPOPT, use similar regularization techniques to numerically remove the singular parts of the Jacobian matrix. However, all these algorithmic solutions require additional computations and may impact the solver's path.

The best option is to reformulate the model to avoid degenerate equations under these situations, such as in the MESH model with bypass in Section 4.3. Alternately unused equipment can be pruned from the flowsheet between solves. This is included in the initialization framework as an optional step.

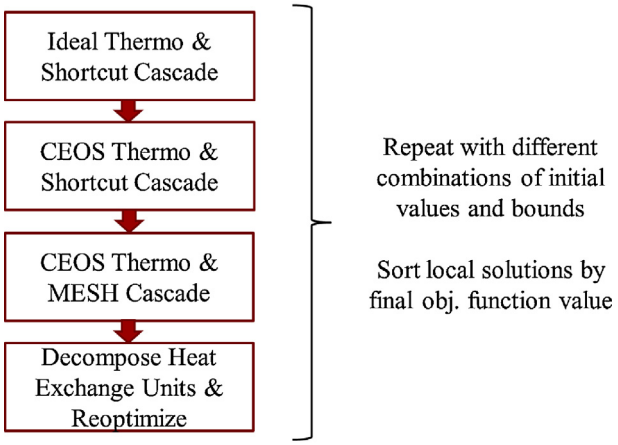

Fig. 8. Initialization procedure.

6.3. Multistart initialization

Experience has shown many local solutions exist for these non-convex flowsheet problems, and the solutions are organized in clusters. Within each cluster the solutions typically share a common topology. Empirical evidence has shown the choice of several initialization parameters including lower bounds, flowsheet pruning strategies and initial variable values dictate in which cluster the optimization algorithms find a solution. Key initialization parameters for the ASU case study are shown in Table 9 (see Supplemental Material). For each combination of parameter levels the the sequence of flowsheet NLPs illustrated in Fig. 8 is solved (in parallel). This provides a practical alternative to global optimization (Tawarmalani and Sahinidis, 2005; Misener and Floudas, 2013), which still remains challenging for large, highly nonlinear, nonconvex flowsheet models.

7. Air separation unit optimization case study

Purification of air into O_2, N_2, and Ar has many industrial applications, ranging from medical supplies to metallurgical processing. Next generation coal power plants with carbon capture may also use O_2 enriched streams for increased efficiency compared to post-combustion capture designs. For example, in oxycombustion power plants coal is combusted in a N_2 lean environment, producing CO_2, water and some pollutants. This effluent requires significantly less processing and purification than traditional coal power plants to prepare the CO_2 for enhanced oil recovery and sequestration (N_2 has already been removed). In this case study, the framework is used to synthesize optimal cryogenic air separation units for coal oxycombustion power plants.

After more than a century the original mechanism for separating large quantities of air remains: distillation at cryogenic temperatures (Foerg, 2002). Typically two or three coupled, heat integrated columns are used for the separation. Air is first compressed at room temperature, cooled and throttled to produce additional cooling via the Joule–Thomson effect. The air is fed into a high pressure column, producing N_2 rich distillate and O_2 rich bottoms. These streams are throttled and fed into a lower pressure column for additional separation, resulting in high purity N_2 and O_2 product streams. An optional third column is used to produce especially high purity gases and/or Ar as a product.

Economic operation of cryogenic air separation units requires tight heat integration to minimize the compressor energy requirement (used to drive the refrigeration cycle). Two strategies are typically employed: (1) the cold product streams cool the warm feed air to cryogenic temperatures in one or more multistream heat exchangers; and, (2) heat from the condensing N_2 rich vapor in the

high pressure column's condenser is used to vaporize high purity O_2 in the low pressure column's reboiler. With advanced designs these linked reboiler-condenser heat exchangers require a driving force temperature difference as small as 0.4 K (Castle, 2002). Despite these efficiency improving measures, cryogenic air separation remains energy intensive, requiring 4.7 times more energy than the theoretical minimum (Fu and Gundersen, 2012).

A variety of approaches have been made to improve cryogenic air separation process efficiencies. Numerous engineers have focused on improvements in equipment design, allowing for smaller minimum driving forces in heat integration equipment, reduced losses in compressors and expanders and lower pressure drops enabled by high efficiency structured packing materials (Foerg, 2002). Other researchers have focused on tailoring air separation units to specific applications. For example, Fu and Gundersen (2012) have applied exergy analysis methods to identify efficiency losses in air separation units for coal oxy-combustion power plants. Jones et al. (2011) compared various ASU configurations for Integrated Gasification Combined Cycle (IGCC) coal power plants by manually adjusting the flowsheet in AspenPlus. Similarly researchers at Air Liquide have used optimization methods to improve ASU designs for oxy-combustion, but offer no algorithm specifics (Darde et al., 2009). Zhu et al. (2010, 2011) apply EO methods with decomposition techniques and large scale NLP solvers to design ASUs under uncertainty. In their study the ASU configuration and number of trays are fixed. The goal of this case study is to demonstrate the effectiveness of EO methods coupled with detailed thermodynamics, new distillation models, simultaneous heat and flowsheet optimization, and large scale NLP algorithms.

The remainder of the case study is organized as follows. First the optimal design problem formulation is stated along with the air separation unit superstructure. Next, detailed flowsheet results are described with the optimal column configuration highlighted. The heat integration results are then discussed and compared with literature, and a sensitivity analysis for O_2 purity is presented. Finally, verification with AspenPlus is considered and numerical performance metrics are disclosed.

7.1. Problem formulation

In this case study ASU specific energy is minimized to produce at least 95 mole% oxygen, a specification common for oxycombustion designs (Fu and Gundersen, 2012; Matuszewski, 2010). In future work, the oxygen purity constraint will be removed as O_2 purity becomes a decision variable in the full power plant optimization problem (along with capital costs). In the problem statement below some equations are deactivated in accordance with the initialization procedure described in Section 6.

Minimize Specific Compression Energy (kWh/kg O_2)

s.t.	Flowsheet Connectivity	Fig. 9
	Stream Models	Eqs. 2 – 4
	Thermodynamics Models	Eqs. [6 – 14, 26 – 29] or [6, 15 – 24, 26 – 27, 113 – 121]
	Equipment Models	Eqs. 32 – 44
	Distillation Cascade Models	Eqs. [45 – 65] or [66 – 67, 74 – 89]
	Heat Integration Models	Eqs. 90 – 101, 104 – 110
	Objective Function Calculations	Eqs. 111 – 112
	O_2 Purity $\geq$ 95 mol%	

Compressor energy is calculated using the ideal gas formula shown in Eq. (111). For this calculation we select $N^{cmpr} = 3$ stages in series with intercooling to 300 K, since optimum compression stages and capital costs are beyond the scope of this case study. Only energy usage is considered in the objective function.

$$E_{sf}^{cmpr} \sum_{s^* \in \{FeedStr\}} f_{s^*,O_2} = F_{sf} N^{cmpr} \frac{\gamma}{\gamma - 1} R \frac{300\text{K}}{1.152 \times 10^5 \,\text{J tonne/kWh}} \times \left[\left(\frac{P_{sf}}{1\text{bar}} \right)^{\gamma - 1/\gamma N^{cmpr}} - 1 \right] \forall s^f \in \{FeedStr\} \tag{111}$$

$$\text{obj.func.} = \sum_{s \in \{FeedStr\}} E_s^{cmpr} + C^{\perp}(\rho^V + \rho^L) + Q^s + Q^w \tag{112}$$

The thermodynamic complementarity constraints (Eqs. (1d) and (1e)) are reformulated (Eqs. (26) and (27)) and included as penalty terms ρ^V and ρ^L in the objective function (Eq. (112)), along with the minimum utility loads (Q^s,Q^w) and compression energy. $C^{\perp}$ (10 to 1000) is a weight for the complementarity penalties. For the best ASU solutions $\rho^V = \rho^L = Q^s = Q^w = 0$; there are no thermodynamic complementarity violations and no external heating or cooling is required.

7.2. ASU superstructure

The superstructure shown in Fig. 9 allows for many common ASU configurations (Castle, 2002; Jones et al., 2011) to be considered. In the superstructure each column is decomposed into two cascade sections (rectifying and stripping). Flash vessels represent trays where feeds are allowed. To accommodate different configurations each feed stream is split and allowed to enter the columns on the first, last and/or an intermediate tray (flash vessel). The number of trays in the cascade sections are variable (but $\geq$2 for the shortcut model), and feed tray location is an optimization variable. The superstructure is formulated with only continuous variables to simplify the optimization problem.

7.3. Optimal double column configuration

One of the best local solutions from the optimization procedure is shown in Fig. 10 and has moderately small columns compared to other ASU designs; there are only 10 and 21 theoretical stages in the high (bottom) and low (top) pressure columns, respectively. This is expected as ASUs are typically designed for high O_2 purity (99.9 + mole%) applications. In the optimized design 91.6% of the feed air is compressed to 3.5 bar, partially liquefied in the multistream heat exchanger and fed into the bottom tray of the high pressure column. The bottom of the HPC produces an oxygen enriched liquid stream (63.5 mol% N_2, 35.0% O_2, 1.5% Ar) at 93.2 K. This stream is throttled to near atmospheric pressure, vaporizing 12.3% and decreasing its temperature to 80.7 K. The stream is fed into the bottom and middle of the low pressure column. The distillate of the high pressure column is a nitrogen rich (98.4% N_2,

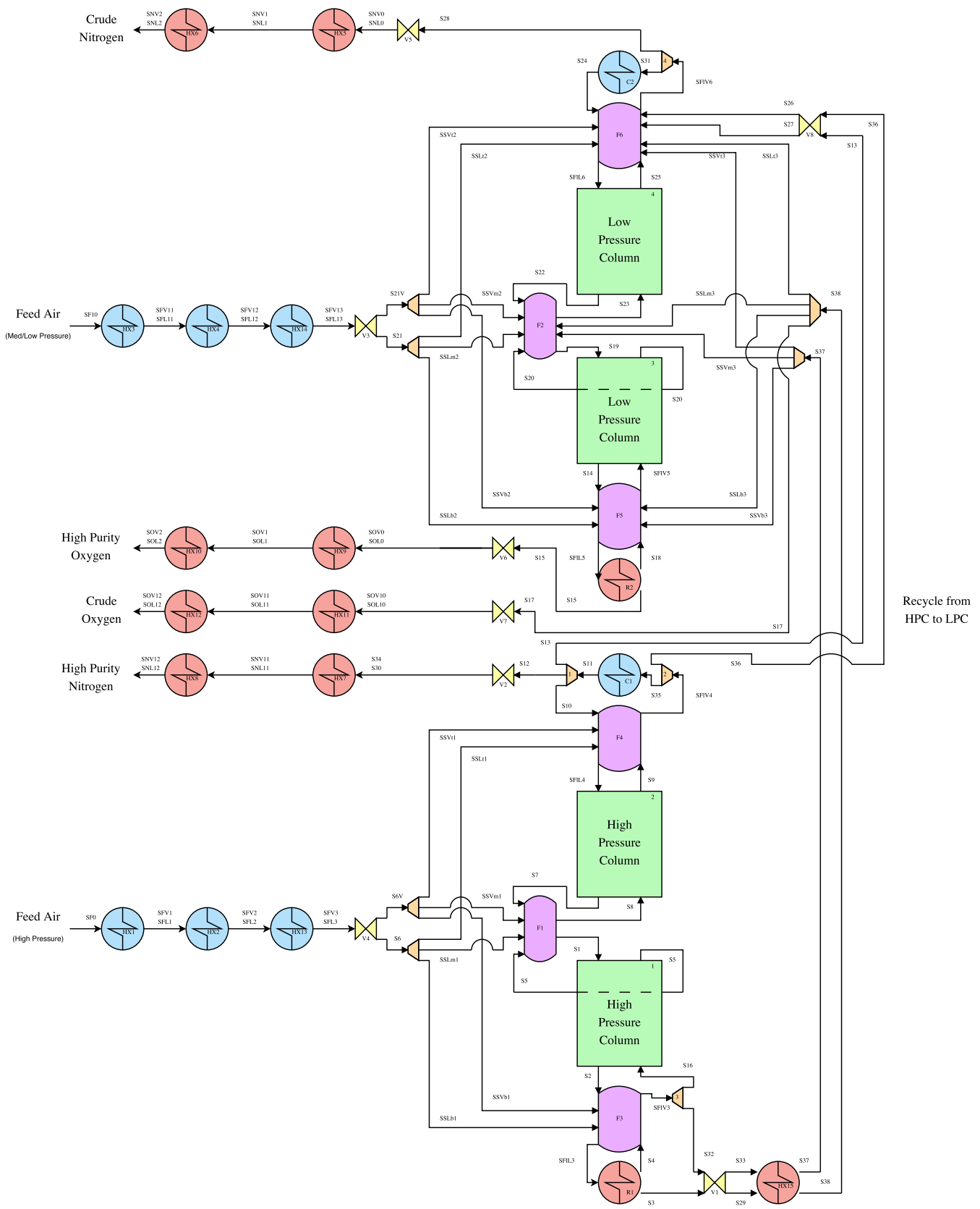

Fig. 9. ASU flowsheet superstructure.

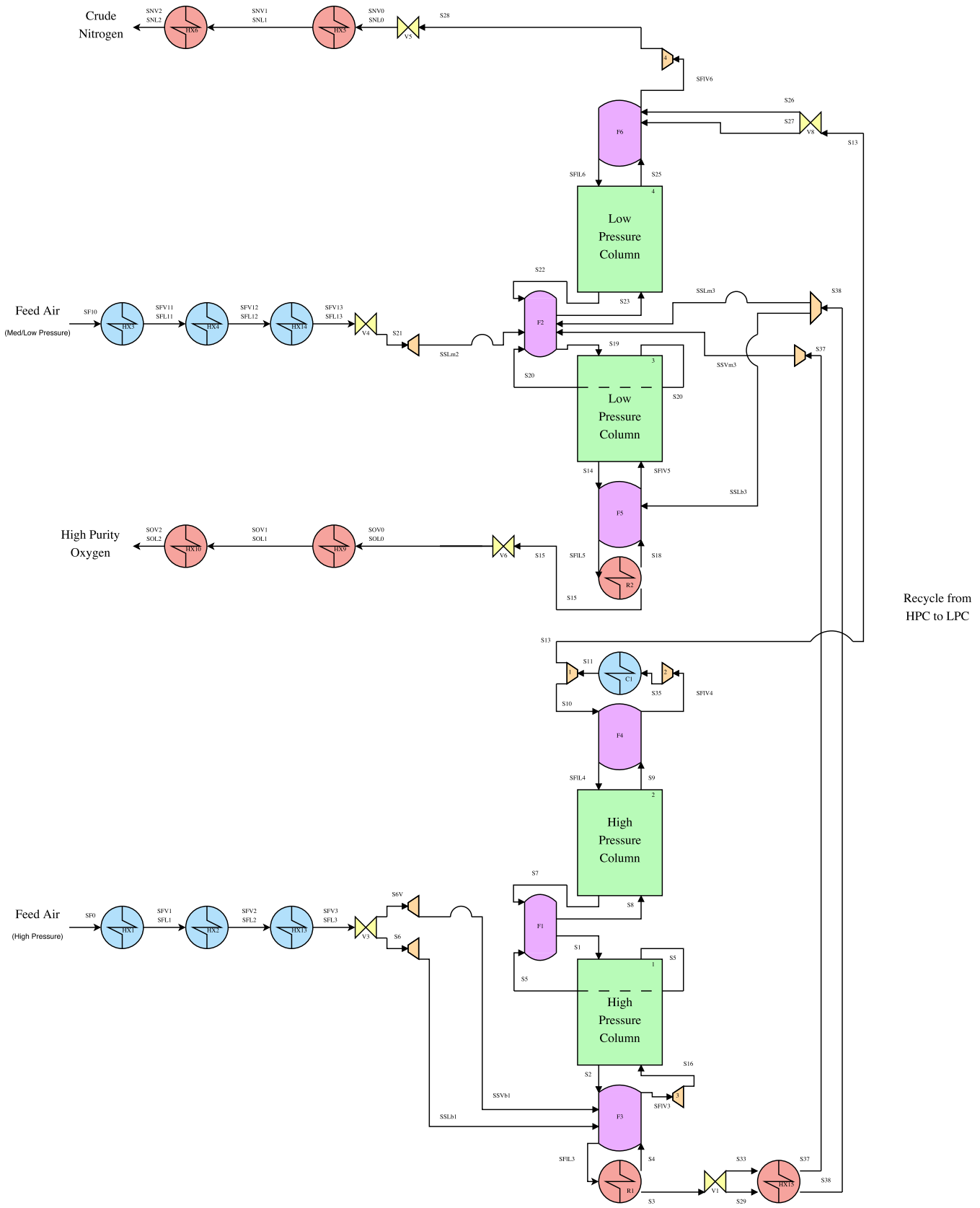

Fig. 10. Optimal ASU topology with ΔT^{min} = 1.5 K, 95% O_2 purity, 0.196 kWh/kg (86% eff. ideal gas compressors).

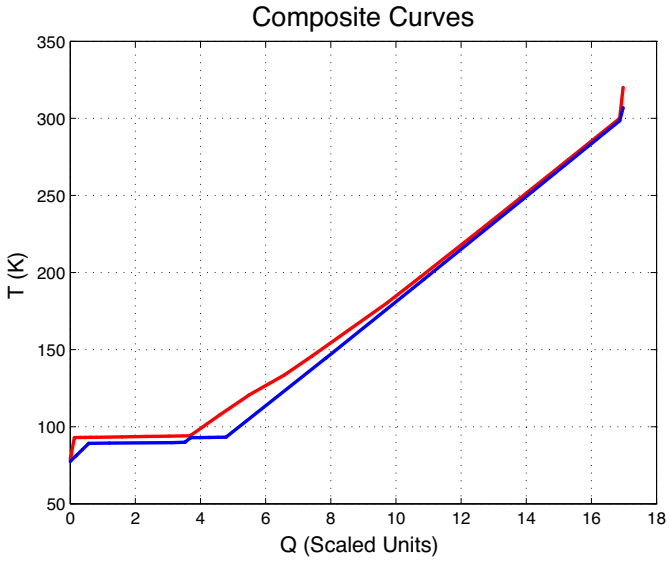

Fig. 11. Composite curves for optimal ASU (Fig. 10) with ΔT^{min} = 1.5, 95% O_2 purity.

1.3% O_2, 0.3% Ar) liquid at 89.7 K. This stream is recycled to the top of the low pressure column, providing reflux and eliminating the need for a LPC condenser.

The remaining 8% of the feed air is compressed to 40 bar, cooled from 320 K to 79.1 K (all liquefied) and fed into the 8th tray (from the bottom) of the low pressure column. The low pressure column produces oxygen product (2.4% N_2, 95.0% O_2, 2.6% Ar) at 89.6 K resulting in 98.0% O_2 recovery from the air feed streams. The HPC distillate is the nitrogen product (98.9% N_2, 0.5% O_2, 0.6% Ar), which is produced at 77.5 K as a vapor. Detailed stream information is included in the supplemental material.

7.4. Heat integration results

Using the models discussed in Section 5, we consider simultaneous heat integration and process optimization. The composite curves, shown in Fig. 11, reveal the process is tightly heat integrated and with no external heating or cooling required ($Q^w = Q^s = 0$). This last point is especially important, as it means cooling from product streams and the Joule–Thomson effect is sufficient to maintain cryogenic operating temperatures at steady-state. Multiple pinch points in the composite curves make the process challenging to heat integrate.

Phase transitions are accommodated using multiple heat exchangers in series, as discussed in Section 5.4 and shown in Fig. 9. Using only the heat exchangers shown in the superstructure, the process was optimized with ΔT^{min} = 1.5 K for the multistream heat exchangers. The linked condenser-reboiler is heat integrated separately with ΔT^{min} = 0.4 K as suggested by Castle (2002). As discussed in Section 5.4 each heat exchange unit is decomposed into 4 subunits with equal temperature spacing and the flowsheet is reoptimized to mitigate constant heat capacity assumption errors. Empirically we found that 4 subunits per heat exchanger balance accuracy with computational costs. Moreover, with 5 or more subunits, we observed little change in the composite curves or energy requirements. The composite curves in Fig. 11 include 4 subunits for all shown heat exchangers, reboilers and condensers.

7.5. Comparison with literature

We compare these results with two optimized designs by Air Liquide described in Matuszewski (2010). The first design is a low capital case with a specific energy usage of 225 kWh/ton (248 kWh/tonne) of O_2 product. The second design is optimized with a low energy usage of 167 kWh/ton (184 kWh/tonne). Although their report includes approximate capital costs, it does not indicate ΔT^{min} used to design the heat exchangers. To compare with the NETL report, the ASU models in this paper are reoptimized at various ΔT^{min} values. Next a polytropic compressor efficiency of 86% is assumed for the designs in Matuszewski (2010). Although this efficiency is not explicitly stated in the report, it is consistent with other NETL studies. The specific energies with compressor inefficiencies are shown in Fig. 12. Our energy performance corresponds with the reported low energy and low capital designs with ΔT^{min} of 1.3 K and 2.8 K, respectively.

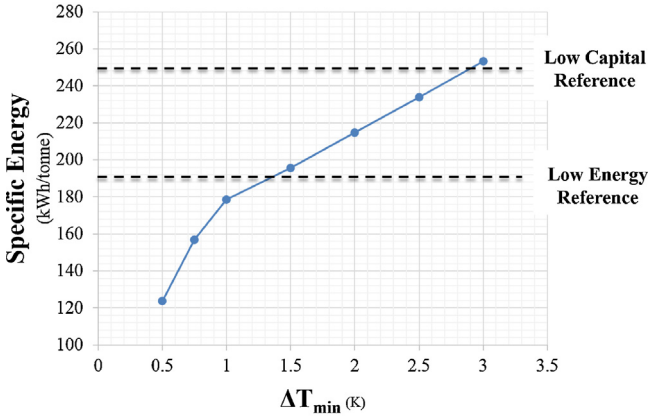

Fig. 12. Optimal ASU designs with various ΔT^{min} specification, 95% O_2 purity product and 86% polytropic efficient compressors.

7.6. Oxygen purity sensitivity

In future work O_2 purity will be considered as an optimization variable instead of a fixed value. This will allow separation efficiency of the ASU and carbon dioxide processing unit (CPU) to be balanced in the full power plant optimization problem. The O_2 purity specification is varied and the ASU flowsheet is reoptimized using the multistart procedure discussed in Section 6, producing the Pareto optimal frontier shown in Fig. 13. This demonstrates the flexibility of the ASU model for future full power plant optimization studies.

A benefit to the equation oriented approach is the availability of sensitivity information at the optimal solution. The KKT multipliers provide a linearized sensitivity of the objective function to perturbations for each constraint and bound. This type of sensitivity

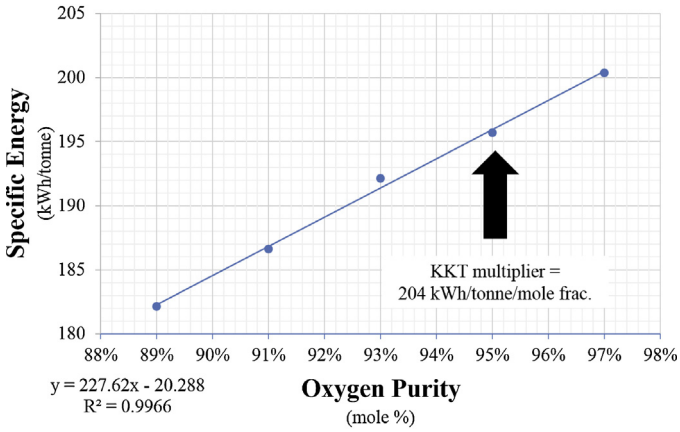

Fig. 13. Optimal ASU designs at various O_2 purities with ΔT^{min} = 1.5 K and 86% polytropic efficient compressors.

Table 3
Comparison of flash calculation outlet streams.

	LPC Top Tray			LPC Reboiler		
	GAMS	Aspen		GAMS	Aspen	
SFlL6	0.9663	0.9713	x_{N_2}	0.0240	0.0241	S15
	0.0199	0.0184	x_{O_2}	**0.9500**	**0.9496**	
	0.0220	0.0103	x_{Ar}	0.0136	0.0263	
Common	77.53	77.85	T (in K)	89.57	89.54	Common
	1.010	1.010	P (in bar)	1.0532	1.0532	
	0.7030	0.6954	Vapor fraction	0.7203	0.7203	
	0	0	Heat duty (kJ/time)	7.848	7.468	
SFlV6	**0.9890**	**0.9908**	y_{N_2}	0.0874	0.0873	S18
	0.0054	0.0051	y_{O_2}	0.8765	0.8767	
	0.0056	0.0041	y_{Ar}	0.0361	0.0360	

is valuable for identifying influential assumptions and parameters that guide more detailed analysis (i.e. generation of a Pareto frontier). As a consistency check the KKT multiplier for the O_2 purity constraint (204 kWh/tonne O_2/mole fraction) is compared with the slope of the linear regression fit through the Pareto curve (228 kWh/tonne/mole frac) and found to be consistent.

7.7. Verification with Aspen Plus®

In order to validate the thermodynamic mode, optimization results are compared against Aspen Plus® simulations for the low pressure reboiler and low pressure column top tray for an ASU design. Both the GAMS optimization results and Aspen verification use the Peng-Robinson equation of state. For both units, the outlet pressure and inlet stream properties (mole fractions, molar flowrate, vapor fraction and pressure) are specified in Aspen Plus to match the optimization results. For the reboiler, the outlet vapor fraction is specified and the heat duty is calculated. For the top tray, adiabatic operation is specified and the vapor fraction is calculated. Outlet stream compositions and temperatures are compared in Table 3 and found to match between GAMS and Aspen. Compositions of the N_2 and O_2 products are shown in bold font. The largest discrepancy is seen with the prediction of bubble and dew point temperature. This is most likely due to differences in the thermodynamic input data (e.g. binary interaction parameters). The heat duties reported in Table 3 assume a basis of 2 mol/time of air into the ASU (consistent with Table 10 in the Supplemental Material). Overall, this comparison confirms the CEOS are correctly implemented in GAMS and leads to confidence in the optimization results.

7.8. Numerical performance

228 starting points were considered for the base case ASU (ΔT^{min} = 1.5 K, 95% O_2 purity) in order to quantify the performance of the multistart initialization procedure outlined in Section 6. 72% of these points produced feasible designs with both negligible thermodynamic complementarity violations and external utility loads (Q^s, Q^w). Additional data are in the supplemental material. For these designs, the sequence of NLPs described in Fig. 8 and the supplemental material took 15 CPU-minutes to complete on average, using 2.4 GHz Intel Xeon processors (one thread per starting point) running Ubuntu Linux. The CONOPT solver (version 3.15I, available in GAMS version 24.0.2) was used to solve the NLPs. Refinements of the initialization procedures could result in further speedups. The best 50 locally optimal solutions' objective function values are within 5% of the best solution's objective function value.

Although it is possible to obtain local solutions with partial bypass fractions using the new MESH model, this is not common. The reason is that partial bypass requires mixing, which is thermodynamically inefficient. Thus solutions with partial bypass (mixing) should require more separation energy. In the ASU case study, we found the best 20 solutions (out of 288 initial points considered) all had integer solutions for the number of trays. Furthermore in the best 150 solutions (150/288 = 52.1%), only 11 (11/150 = 7.3%) have partially bypassed trays.

Quantifying problem size is difficult given the complex initialization strategy. Each NLP in the initialization procedure may have a different size depending on the initial point, the equipment set pruned and the number of MESH trays considered. For the final NLP of the solution reported in Fig. 10, there are 15,893 equations (14,615 equality constraints, 282 active inequality constraints and 996 inactive inequality constraints) and 15,534 variables. 574 variable bounds are strongly active at the solution resulting in 261 degrees of freedom with the active set selected by CONOPT.

8. Conclusions and future work

We present a new framework for advanced equation-oriented (EO) flowsheet optimization. By leveraging automatic differentiation, first and second derivatives are exactly (and efficiently) calculated, enabling the use of high performance large scale nonlinear programming algorithms. Along with careful problem formulation, these algorithms support optimization of complex flowsheets with detailed first principle models.

Two themes are embodied throughout the framework. First each main model is built up from simple to complex in order to form a comprehensive initialization and assumption verification strategy. Second the modeling framework is designed to be modular, allowing for easier extension. Generalized types of units are introduced (general thermodynamic equipment, general heat exchanger units) and common equations are inherited from these general types to form specific equipment models (flash vessel, heat exchanger, etc.)

These two themes are seen in the three main models discussed. Two thermodynamics modules, simple correlation based and more detailed cubic equation of state, introduced in Section 2. Both modules use complementarities to relax phases, which are shown to be equivalent to local Gibbs free energy minimization for phase calculations. Similarly two distillation cascade models are presented in Section 4. The first is an extension of the Kremser–Edmister shortcut method and the second is a novel MESH formulation with tray bypass. Both of these models allow for the optimization of distillation column size, flowrates, temperatures, pressures and tray location without discrete variables, greatly simplifying the optimization problem. The new MESH formulation with tray bypass provides well defined behavior for partial stages. Finally an extension of the Duran–Grossmann heat integration model is presented in Section 5. This allows for simultaneous heat integration and flowsheet optimization without design of the heat exchanger network (thus avoiding discrete variables). Phase changes and non-constant heat capacities are considered with multiple heat exchangers in series and decomposition of heat exchange units into 4 subunits.

The new framework is demonstrated by designing an Air Separation Unit (ASU) for advanced coal combustion power plants in Section 7. ASU design is particularly difficult due to the tight heat integration and numerous viable system configurations. Multistream heat exchanger design is considered inside the flowsheet optimization problem using the pinch based heat integration formulation. Several popular configurations from literature are realizable using the ASU superstructure. Optimization leads to a minimum specific energy for separation of 0.196 kWh/kg of O_2 with ΔT^{min} = 1.5 K for the multistream heat exchanger, 95 mol% O_2 purity product specification and 86% polytropic efficient compressors. ΔT^{min} is estimated for two designs in literature using the optimization framework. Moreover, the ASU designs require no external utilities ($Q^s = Q^w = 0$) and the constant heat capacity assumption for heat integration is verified by decomposing heat exchange unit into subunits. The case study offers insights into the best configurations for next generation coal power plant applications and demonstrates the effectiveness of the new framework on challenging process synthesis problems.

Ultimately the optimization framework will be extended to consider optimization of an entire coal oxycombustion power plant flowsheet as part of the Carbon Capture Simulation Initiative sponsored by the US Department of Energy. Development of optimization-friendly models for steam turbines, oxycombustion boilers, and CO_2 processing units is already underway. Simultaneous optimization of the entire flowsheet will enable complex trade-offs to be considered, including integration opportunities between the cryogenic ASU and cryogenic CO_2 processing unit. Flexibility of the ASU model and optimization framework is demonstrated by reoptimizing the ASU for different O_2 purity specifications. The ASU case study will also be extended in the future to include capital costs, double reboiler configurations and pressure drops in heat exchangers.

Acknowledgements

This article was prepared as an account of work sponsored by an agency of the United States Government. Neither the United States Government nor any agency thereof, nor any of their employees, makes any warranty, express or implied, or assumes any legal liability or responsibility for the accuracy, completeness, or usefulness of any information, apparatus, product, or process disclosed, or represents that its use would not infringe privately owned rights. Reference herein to any specific commercial product, process, or service by trade name, trademark, manufacturer, or otherwise does not necessarily constitute or imply its endorsement, recommendation, or favoring by the United States Government or any agency thereof. The views and opinions of authors expressed herein do not necessarily state or reflect those of the United States Government or any agency thereof.

Appendix A. Supplementary Data

Supplementary data associated with this article can be found, in the online version, at http://dx.doi.org/10.1016/j.compchemeng.2014.05.013.

References

Andrecovich MJ, Westerberg AW. An MILP formulation for heat-integrated distillation sequence synthesis. AIChE J 1985;31(9):1461–74.
Biegler LT. Nonlinear programming: concepts, algorithms, and applications to chemical processes. Society of Industrial and Applied Mathematics; 2010.
Biegler LT, Grossmann IE, Westerberg AW. Systematic methods of chemical process design. Upper Saddle River, NJ, USA: Prentice Hall PTR; 1997.
Castle WF. Air separation and liquefaction: recent developments and prospects for the beginning of the new millennium. Int J Refrig 2002;25:158–72.
Darde A, Prabhakar R, Tranier J-P, Perrin N. Air separation and flue gas compression and purification units for oxy-coal combustion systems. Energy Proc 2009;1(1):527–34.
Dowling AW, Biegler LT. Optimization-based process synthesis for sustainable power generation. Chem Eng Trans 2013;35:1–12.
Duran MA, Grossmann IE. Simultaneous optimization and heat integration of chemical processes. AIChE J 1986;32(1):123–38.
Edmister WC. Absorption and stripping-factor functions for distillation calculation by manual- and digital-computer methods. AIChE J 1957;3(2):165–71.
Foerg W. History of cryogenics: the epoch of the pioneers from the beginning to the year 1911. Int J Refrig 2002;25:283–92.
Fu C, Gundersen T. Using exergy analysis to reduce power consumption in air separation units for oxy-combustion processes. Energy 2012;44(1):60–8.
Furman KC, Sahinidis NV. A critical review and annotated bibliography for heat exchanger network synthesis in the 20th century. Ind Eng Chem Res 2002;41:2335–70.
Gopal V, Biegler LT. Smoothing methods for complementarity problems in process engineering. AIChE J 1999;45(7):1535–47.
Gundersen T. Numerical aspects of the implementation of cubic equations of state in flash calculation routines. Comput Chem Eng 1982;6(3):245–55.
Jones D, Bhattacharyya D, Turton R, Zitney SE. Optimal design and integration of an air separation unit (ASU) for an integrated gasification combined cycle (IGCC) power plant with CO_2 capture. Fuel Process Technol 2011;92(9):1685–95.
Kamath RS, Biegler LT, Grossmann IE. An equation-oriented approach for handling thermodynamics based on cubic equation of state in process optimization. Comput Chem Eng 2010;34(12):2085–96.
Kamath RS, Biegler LT, Grossmann IE. Modeling multi-stream heat exchangers with and without phase changes for simultaneous optimization and heat integration. AIChE J 2012;58(1):190–204.
Kamath RS, Grossmann IE, Biegler LT. Aggregate models based on improved group methods for simulation and optimization of distillation systems. Comput Chem Eng 2010;34(8):1312–9.
Knapp H, Doring R, Oellrich L, Plocker U, Langhorst S, Zeck Prausnitz JM. Vapor–liquid equilibria for mixtures of low boiling substances, vol. VI. DECHEMA; 1982.
Kossack S, Kraemer K, Marquardt W. Efficient optimization-based design of distillation columns for homogenous azeotropic mixtures. Ind Eng Chem Res 2006;45(25):8492–502.
Kraemer K, Kossack S, Marquardt W. Efficient optimization-based design of distillation processes for homogeneous azeotropic mixtures. Ind Eng Chem Res 2009;48(14):6749–64.
Linnhoff B. Pinch analysis: a state-of-the-art overview. Trans IChemE 1993;71(A).
Matuszewski M. Cost and Performance for Low-Rank Pulverized Coal Oxycombustion Energy Plants. National Energy Technology Labratory; 2010, Technical Report DOE/NETL-401/093010.
Misener R, Christodoulos A. Floudas ANTIGONE: Algorithms for coNTinuous / Integer Global Optimization of Nonlinear Equations; 2013.
Reid RC, Prausnitz JM, Poling BE. The properties of gases and liquids. 4th edition McGraw-Hill Book Company; 1987.
Reid RC, Prausnitz JM, Sherwood TK. The properties of gases and liquids. 3rd edition McGraw-Hill Book Company; 1977.
Sargent RWH, Gaminibandara K. Introduction: approaches to chemical process synthesis. Optim Action 1976.
Stein O, Oldenburg J, Marquardt W. Continuous reformulations of discretecontinuous optimization problems. Comput Chem Eng 2004;28(10):1951–66.
Tawarmalani M, Sahinidis NV. A polyhedral branch-and-cut approach to global optimization. Math Program 2005;103:225–49.
Viswanathan J, Grossmann IE. A combined penalty function and outer-approximation method for MINLP optimization. Comput Chem Eng 1990;14(7):769–82.
Viswanathan J, Grossmann IE. An alternate MINLP model for finding the number of trays required for a specified separation objective. Comput Chem Eng 1993a;17(9):949–55.
Viswanathan J, Grossmann IE. Optimal feed locations and number of trays for distillation columns with multiple feeds. Ind Eng Chem Res 1993b;32:2942–9.
Yeomans H, Grossmann IE. Disjunctive programming models for the optimal design of distillation columns and separation sequences. Ind Eng Chem Res 2000a;39(6):1637–48.
Yeomans H, Grossmann IE. Optimal design of complex distillation columns using rigorous tray-by-tray disjunctive programming models. Ind Eng Chem Res 2000b;39(11):4326–35.
Zhu Y, Legg S, Laird CD. Optimal design of cryogenic air separation columns under uncertainty. Comput Chem Eng 2010;34(9):1377–84.
Zhu Y, Legg S, Laird CD. Optimal operation of cryogenic air separation systems with demand uncertainty and contractual obligations. Chem Eng Sci 2011;66(5):953–63.